

Historical and projected changes in the Southern Hemisphere surface westerlies

Rishav Goyal¹, Alexander Sen Gupta¹, Martin Jucker¹, and Matthew H. England¹

¹University of New South Wales

November 21, 2022

Abstract

Changes to the Southern Hemisphere (SH) surface westerlies not only affect air temperature, storm tracks and precipitation; they are also pivotal in controlling global ocean circulation, ocean heat transport, and ocean carbon uptake. Wind-forced ocean perturbation experiments have commonly applied idealized poleward wind shifts ranging between 0.5 and 10 degrees of latitude, and wind intensification factors of between 10 and 300%. In addition, changes in winds are often prescribed ad-hoc without consistently accounting for physical constraints and can neglect important regional and seasonal differences. Here we quantify historical and future projected SH westerly wind changes based on examination of CMIP5, CMIP6 and reanalysis data. Under a high emission scenario, we find a projected end of 21st Century annual mean westerly wind increase of ~10% and a poleward shift of ~0.8° latitude, although there are also significant seasonal and regional variations.

1 **Historical and projected changes in the Southern Hemisphere**
2 **surface westerlies**

3

Rishav Goyal^{1,2,*}, Alex Sen Gupta^{1,2}, Martin Jucker^{1,2} and Matthew H. England^{1,2}

1. Climate Change Research Centre, University of New South Wales, NSW, 2052 Australia

2. ARC Centre of Excellence for Climate Extremes, University of New South Wales, NSW,
Australia

4

5

6

7

8

9

10 **Corresponding author: rishav.goyal@unsw.edu.au*

11

12

13 **Key points**

14 1. Recent observational record is dominated by internal variability and is not a good

15 indicator of forced changes in the westerlies

16 2. With reduced mean state biases compared to CMIP5, CMIP6 models provide a more

17 credible estimate of past and future changes in surface westerlies.

18 3. There are significant regional and seasonal differences in wind changes that need to be

19 considered when simulating past and future trends

20

21

22 **Abstract**

23 Changes to the Southern Hemisphere (SH) surface westerlies not only affect air
24 temperature, storm tracks and precipitation; they are also pivotal in controlling global ocean
25 circulation, ocean heat transport, and ocean carbon uptake. Wind-forced ocean
26 perturbation experiments have commonly applied idealized poleward wind shifts ranging
27 between 0.5 and 10 degrees of latitude, and wind intensification factors of between 10 and
28 300%. In addition, changes in winds are often prescribed ad-hoc without consistently
29 accounting for physical constraints and can neglect important regional and seasonal
30 differences. Here we quantify historical and future projected SH westerly wind changes
31 based on examination of CMIP5, CMIP6 and reanalysis data. Under a high emission scenario,
32 we find a projected end of 21st Century annual mean westerly wind increase of ~10% and a
33 poleward shift of ~0.8° latitude, although there are also significant seasonal and regional
34 variations.

35

36 **Plain Language Summary**

37 The westerly winds in the Southern Hemisphere have increased in speed and shifted
38 towards Antarctica in the last few decades, and these are projected to intensify and move
39 further poleward in the future. Changes in the westerly winds are of great importance
40 because they control ocean carbon uptake, ocean circulation and ocean heat transport. To
41 understand the impacts of changes in the westerlies on the Southern Ocean, ocean model
42 simulations are often run by artificially increasing and shifting winds towards Antarctica to
43 approximate future changes in the winds. However, there is no consistency in the way these
44 changes are incorporated, with large variations in the applied shift and strengthening. In this
45 study, we quantify recent observed and projected changes in the surface westerlies, aiming

46 to provide guidance as to what wind perturbations should be applied in ocean models. We
47 further show that the latest generation of coupled climate models provides a more credible
48 estimate of past and future changes in the surface westerly winds.

49

50

51

52 **1. Introduction**

53 The Southern Hemisphere (SH) surface westerlies are the strongest time averaged surface
54 winds on the planet. The surface westerlies affect the distribution of clouds, precipitation
55 and the position and intensity of storm tracks in the Southern Hemisphere high latitudes
56 (e.g. Bracegirdle, 2013; Thompson et al., 2011) . Changes in these westerlies also have a
57 strong imprint on ocean circulation including the Atlantic Meridional Overturning (Hall &
58 Visbeck, 2002; Toggweiler et al., 2006; Waugh et al., 2013), water mass formation (Oke &
59 England, 2004), Antarctic sea-ice and ice shelves (Holland et al., 2019) , oceanic uptake of
60 heat and carbon (Sen Gupta & England, 2006; Lovenduski et al., 2007; Le Quere et al., 2007)
61 and future changes in the western boundary current extensions (H. Yang et al., 2016) .

62

63 The surface westerlies in the SH mid-latitudes have intensified and shifted poleward over
64 the past few decades through the combined influence of an increase in greenhouse gases
65 and stratospheric ozone depletion (Arblaster & Meehl, 2006; Thompson et al., 2011), with
66 the latter thought to be the dominant driver for the recent poleward intensification (Roscoe
67 & Haigh, 2007; Drew T Shindell, 2004; Thompson, 2002). While ozone concentrations are
68 expected to recover in the future, the westerly winds are projected to continue to shift
69 poleward and intensify based on high emission climate model experiments. Under these

70 conditions, the effect of greenhouse gases is expected to dominate the opposing influence
71 of ozone recovery (Thompson et al., 2011). Hence, understanding the impact of changing
72 westerly winds on the ocean circulation remains an ongoing focus of research.

73

74 Several studies using ocean and coupled climate models ranging from coarse to eddy
75 permitting resolutions have been conducted in the past to understand the influence of
76 projected 21st Century poleward intensification of the surface westerlies on the Southern
77 Ocean and Antarctica (e.g. Delworth & Zeng, 2008; Frankcombe et al., 2013; Spence et al.,
78 2014). Most of these studies apply an idealized zonally symmetric intensification and/or
79 poleward shift in the westerly winds in the SH extratropics (generally between 40-60°S).
80 These prescribed changes cause significant impacts on various features of the SH, including
81 the distribution of projected sea level rise (Frankcombe et al., 2013), subsurface warming
82 and circulation changes around the Antarctic continental margin (Spence et al., 2014).
83 However, the applied wind changes tend to be idealized and *ad hoc*, with no common
84 protocol for applying these wind perturbations to ocean models, including the chosen
85 magnitude of the wind shift and its intensification.

86

87 To examine the effect of future changes in surface westerlies, previous studies have applied
88 a broad range of poleward shifts and intensifications, with the poleward shift ranging
89 between 0.5 and 10 degrees latitude and wind intensification factors ranging from 10 up to
90 300%, and sometimes more. Given the wide range of perturbations that have been applied
91 in past studies, some guidance regarding a reasonable estimate of the past and projected
92 changes in the location and strength of the westerly winds in the SH is needed to better
93 facilitate model intercomparison.

94

95 In this study, we analyze the historical and projected intensification and poleward shift in
96 the SH surface westerlies across an ensemble of models from the Coupled Model Inter-
97 comparison Project 5 & 6 (CMIP5 and CMIP6) along with reanalysis products. We also
98 examine the seasonality and regional variations in these wind stress changes. These details
99 are important for correctly simulating certain aspects of change in the ocean and in
100 Antarctic sea ice. We also examine whether reanalysis products can be used to provide a
101 reliable estimate of the forced anthropogenic change in SH surface westerlies over the last
102 few decades.

103

104 **2. Data and Methods**

105 Surface monthly averaged zonal winds (at 10m elevation) from the CMIP5 and CMIP6
106 archives as well as reanalysis products are used to examine the latitude and strength of the
107 SH surface westerlies. Ocean model simulations employ surface winds to calculate both the
108 surface wind stress and air-sea turbulent heat fluxes; both are primary boundary conditions
109 for ocean models. Surface winds also determine sea-ice advection and wind-driven mixed
110 layer deepening and are therefore central to ocean-sea-ice model forcing fields.

111

112 Data spanning 1850 through to 2099 from the first ensemble from each of multiple CMIP5
113 and CMIP6 models are used to provide equal weight to each climate model. Data from pre-
114 industrial control simulations (200-year runs from 27 CMIP5 and 23 CMIP6 models),
115 historical simulations (1850-2005 for CMIP5 and 1850-2014 for CMIP6) and future
116 projections (2006-2099 for CMIP5 and 2015-2099 for CMIP6) are used in this study (Table
117 S1, S2). For the future projections, data from both the intermediate emissions scenario

118 (Representative Concentration Pathway (RCP) 4.5 for CMIP5 and the Shared Socio-economic
119 Pathway (SSP) 245 for CMIP6) and the high emissions scenario (RCP8.5 for CMIP5 and
120 SSP585 for CMIP6) are analyzed. Both SSP585 (SSP245) and RCP8.5 (RCP4.5) scenarios are
121 designed so that radiative forcing increases by 8.5W/m^2 (4.5W/m^2) by 2100 relative to pre-
122 industrial, although the emission rates of various greenhouse gases are different while
123 achieving the same radiative forcing by 2100 (O'Neill et al., 2016). The differences in high
124 emissions and moderate emissions scenarios arise because of differences in the projected
125 concentrations of greenhouse gases, aerosols and stratospheric ozone.

126

127 Reanalysis datasets from 1979-2019 for monthly averaged surface zonal winds (at 10m
128 elevation) from the European Centre for Medium Range Weather Forecasts (ECMWF) Re-
129 analysis (ERA5, Hersbach et al., 2020), and the Japanese reanalysis (JRA-55, Kobayashi et al.,
130 2015) are also analyzed. Because of sparse measurements over the Southern Ocean before
131 the satellite era, reanalysis data before the year 1979 are not considered as they do not
132 provide a reliable estimate of the westerly wind changes over the SH. Even though satellite
133 measurements of winds only started in the late 1980s, satellite measurements of other
134 physical quantities help to appreciably improve the quality of the reanalysis products post
135 1979. Therefore, the reanalysis wind fields from 1979 on are used in this study. Close
136 agreement was found between ERA-5 and JRA-55 for all analyses presented in this study;
137 hence for simplicity we only present results from the ERA5 reanalysis. We also considered
138 the National Centre for Environmental Prediction-National Centre for Atmospheric Research
139 (NCEP-NCAR) reanalysis (Kalnay et al., 1996), however, in agreement with Marshall (2003),
140 we found that this dataset contains spuriously large trends in high latitude Southern
141 Hemisphere winds that are inconsistent with station-based observations. All data are first

142 mapped to a common 1° x 1° latitude-longitude grid before conducting the analyses shown
143 below.

144

145 The maximum jet strength is defined as the maximum surface zonal wind at each longitude
146 in the SH extratropics between 30-70°S (consistent with the definition of Bracegirdle et al.,
147 2013). The position of the westerly jet is then defined as the latitude where the maximum
148 zonal surface wind speed is located at each longitude between 30-70°S.

149

150

151 **3. Historical Era**

152 A poleward intensification of the SH surface westerlies is found over the last few decades in
153 both models and reanalysis (Fig. 1a, 1b). This poleward intensification can be described as a
154 positive trend in the SAM (Fig. S1) over the last few decades. Based on single forcing
155 experiments, this change has been attributed primarily to stratospheric ozone depletion,
156 with greenhouse gases playing a secondary role (Thompson et al., 2011).

157

158 CMIP5 and older generation climate models are known to have a large equatorward bias
159 (Fig. 1a) in the zonal mean location of the SH surface westerlies (Bracegirdle et al., 2013)
160 possibly due to biases in the shortwave cloud forcing in the models as compared to
161 reanalysis (Ceppi et al., 2012). Biases in the shortwave cloud forcing can induce surface
162 temperature anomalies in the midlatitudes which affect the meridional temperature
163 gradient, which in turn affects the mean latitude of the westerlies. Negative biases in
164 shortwave cloud forcing correspond to equatorward biases in the latitude of the westerlies.
165 There is a notable reduction in the equatorward bias (compared to ERA5) in the zonal mean

166 location of the maximum SH surface westerlies (see also Bracegirdle et al., 2020) reducing
167 from 1.3° in CMIP5 models down to 0.3° in the CMIP6 multi-model mean, averaged over
168 1979 to 2005. While the bias has been reduced, two-thirds of models still have a zonal
169 maximum situated further north than the reanalysis estimate (Fig. 1a). In contrast, the
170 CMIP5 multi-model mean (MMM) has an almost identical mean strength for the SH surface
171 westerlies as compared to ERA5, while the CMIP6 MMM is 4% too strong (see Fig. 1b).
172 When limiting this inter-generational CMIP comparison to include just the subset of models
173 that are common to both CMIP5 and CMIP6 (i.e., 12 models; see Table S1, S2), we again find
174 a significant reduction in the equatorward bias (reduced bias of ~0.7° latitude; Fig. S2a). In
175 contrast, we do not find any significant inter-generational difference in the strength of SH
176 surface westerlies between CMIP5 and CMIP6 (Fig. S2b).

177

178 Studies examining the ocean response to historical changes in surface winds usually rely on
179 atmospheric reanalyses for their forcing fields. However, changes over the relatively short
180 reanalysis period may be strongly influenced by internal climate variability and may be a
181 poor representation of the anthropogenic forced change. To test if the trends in the zonal
182 mean location and strength in the ERA5 reanalysis lie outside the range of internal climate
183 variability, a Monte-Carlo analysis was carried out by calculating trends over large numbers
184 of random 41-year periods from the 200-year pre-industrial control simulations of 50 CMIP
185 models (27 CMIP5 and 23 CMIP6; Fig. S3). This test assumes that the model variability is
186 representative of the observed internal climate variability. The trend in the location of the
187 SH westerlies calculated from the ERA5 reanalysis lies well within the distribution of trends
188 associated with internal variability. However, the trend in the strength of the westerlies is
189 unlikely to be explained by internal variability alone ($P < 0.1$). Given the model differences in

190 the representation of internal variability we repeat the analysis using individual CMIP5 and
191 CMIP6 models. Similar results are obtained in more than 90% of the models for both the
192 position and strength of the surface westerlies (Fig. S4-7). A seasonal analysis further finds
193 that trends in both position and strength and for both model generations are significant in
194 summer (DJF, Fig. S8, S9). In all other seasons and for both metrics, the reanalysis trends are
195 within the range expected from internal variability. This is consistent with recent pacemaker
196 model simulations by Schneider et al. (2015) and Yang et al. (2020), who found that a
197 substantial component of recent multi-decadal westerly wind variability could be accounted
198 for in model experiments forced by observed tropical SST variations, independent of
199 anthropogenic forcing.

200

201 Most previous ocean model studies that have examined the effects of SH wind changes
202 have done so by prescribing zonally symmetric changes in wind latitude and strength (e.g.
203 Delworth & Zeng, 2008; Downes et al., 2017; Frankcombe et al., 2013; Hogg et al., 2017;
204 Spence et al., 2014; Waugh et al., 2019). Zonal differences in the changes in SH westerlies
205 has only been examined in a few studies (e.g. Bracegirdle et al., 2013; Waugh et al., 2020).
206 The climatological zonal mean location of the surface westerlies is more poleward in the
207 Pacific and western Indian Ocean compared to the Atlantic and eastern Indian basins (Fig.
208 2a). This is also a consistent feature in the climate models. In the ERA5 reanalysis, there is
209 an 8° meridional difference in the most poleward (~56°S) and equatorward locations (~48°S)
210 of the climatological mean surface westerlies observed over 2000-2019 (Fig. 2a). The CMIP5
211 MMM shows an equatorward bias in the latitude of the westerlies at all longitudes (Fig. 2a)
212 consistent with the zonal average analysis (Fig. 1a). However, consistent with the
213 improvement in the location of the zonal mean climatological surface westerlies, the CMIP6

214 MMM shows a better agreement with the ERA5 reanalysis at almost all longitudes
215 compared to CMIP5 MMM, although biases of up to 0.9° persist in the region centered
216 south of New Zealand (Fig. 2a).

217

218 We next examine recent regional trends in the ERA5 reanalysis to examine whether they
219 can be accounted for by intrinsic variability, or whether they can provide a reliable estimate
220 of the forced signal. To do this, we compute regional trends in the location and strength of
221 surface westerlies in the ERA5 reanalysis, as well as in CMIP5 and CMIP6 models, for the
222 modern period (1979-2019). Major regional differences between ERA5 and modelled trends
223 in the meridional location of the westerlies can be seen (Fig 2b). Regional differences in
224 trends in the meridional location of westerlies from either model generations are not
225 consistent with the ERA5 trends. Indeed, even though the MMM averages over a large
226 component of the internal variability inherent in individual models, we still find no
227 consistency in the regional pattern of trends between the CMIP5 and CMIP6 MMM (Fig 2b).
228 For example, in the east Pacific ERA5 shows a strong positive trend, in contrast to the CMIP5
229 MMM which shows a negative trend and CMIP6 MMM which has almost no trend (Fig. 2b).
230 We conclude that over the relatively short reanalysis period (i.e. 41 years from 1979-2019),
231 the regional differences in trends in both the latitude and the strength of westerlies are
232 likely dominated by natural interannual to decadal climate variability. Indeed, because of
233 large intermodel differences, presumably linked to each model's intrinsic variability, the
234 MMM trends obtained from CMIP5 and CMIP6 are not significant at almost all longitudes
235 (Fig. 2b, 2c).

236

237 For the models we extend the above analysis to cover the full 20th Century, to see if robust
238 regional patterns in the trends emerge. Using the longer period for both the CMIP6 and
239 CMIP5 models, similar regional patterns in MMM trends in the position of westerlies are
240 found, with significant poleward trends identified everywhere except in the western Pacific,
241 (Fig. 3b), with spatial correlation coefficient of 0.7 ($P < 0.05$) between CMIP5 and CMIP6
242 MMM trends. Similar regional patterns are also found in trends in the strength of the
243 westerlies (spatial correlation coefficient of 0.8 ($P < 0.05$) between CMIP5 and CMIP6 MMM
244 trends) with strong trends found in the eastern Indian and western Atlantic Oceans basins
245 (Fig. 3c).

246

247 Changes in the zonal mean position and strength of the westerlies also show consistent
248 seasonal differences over the historical time period (1900-1999, Fig. S10). While a poleward
249 shift is found in all four seasons in both CMIP5 and CMIP6 MMM (Fig. S10a), the strongest
250 trends are found during summer and weakest trends during winter (Fig. S10a). Similar
251 seasonality is also found in the wind strength trends, with stronger trends in summer
252 compared to winter (Fig. S10b).

253

254 **4. Future Projections**

255 Future changes in the SH surface westerlies are expected to be affected by the competing
256 effects of increasing greenhouse gases (GHGs) and stratospheric ozone recovery (Thompson
257 et al., 2011). While both GHGs and ozone have acted in concert in the past, as ozone
258 recovers it is expected that the two effects will tend to cancel each other out in the future
259 (e.g. Eyring et al., 2010; Goyal et al., 2019; Newman et al., 2006). After ozone recovery

260 stabilizes, it is expected that changes in the westerlies will be largely determined by changes
261 in GHGs.

262

263 Projected 21st Century (2000-2099) changes in the high emissions scenario of CMIP5 and
264 CMIP6 show a significant poleward shift (by $\sim 1.5^\circ/100\text{yr}$ latitude in CMIP5 & by $0.8^\circ/100\text{yr}$
265 in CMIP6 MMM) and intensification ($\sim 0.8\text{m/s}/100\text{yr}$ in CMIP6 MMM and $\sim 0.7\text{ m/s}/100\text{yr}$ in
266 CMIP5 MMM) in the zonal mean location and strength of SH westerlies (Fig. 1, Table S3). As
267 with the historical period, there are also major difference in these trends by season (Fig. 4).
268 In particular, a poleward shift is found in all seasons with the largest shift projected during
269 autumn and summer (compared to only in summer during the historical era), and a weaker
270 shift projected for winter and spring (Fig. 4a, Fig. S10a). Strengthening of the westerlies is
271 also projected in all seasons with the weakest trends in summer, in contrast to the historical
272 era, when summertime trends were the strongest (Fig. 4b, Fig. S10b). As discussed earlier,
273 the projected changes in the SH westerlies are expected to be affected by the competing
274 effects of increasing GHGs and stratospheric ozone recovery. While the effect of GHGs acts
275 in all seasons, stratospheric ozone primarily affects the SH during summer because of the
276 breakdown of the stratospheric polar vortex during spring (Arblaster & Meehl, 2006).
277 Weaker summertime trends in the 21st Century are therefore expected because of the
278 opposing contributions of GHGs and stratospheric ozone forcing in that season (Fig. 4). This
279 suggests that the role of GHGs becomes much more important in the future under a high
280 emission scenario, particularly given the expected recovery of stratospheric ozone.
281 Consistent results are found for projected changes in both the latitude and the strength of
282 westerlies in CMIP5 models, although trends are stronger in the CMIP5 MMM (Fig. 4). It is
283 interesting to note that the projected *strengthening* of westerlies in the high emission

284 scenarios of both CMIP5 and CMIP6 models during the 21st Century occurs throughout the
285 year, but is strongest in winter and spring, whereas the projected *shift* in westerlies is
286 considerably larger in summer and autumn compared to winter and spring (Fig. 4). This is
287 counter to the expectation that the changes in the latitude and strength of westerlies
288 operates in tandem (Bracegirdle et al., 2013), suggesting that different factors might be
289 affecting the projected seasonal trends in both the poleward shift and the strengthening of
290 westerlies in the SH.

291

292 In contrast to the high emission scenario, no significant trends are found in the moderate
293 emissions scenario in both CMIP6 (SSP245) and CMIP5 (RCP45) MMM for both the latitude
294 (except during autumn in CMIP5) and strength (except during autumn and spring in CMIP5)
295 of the surface westerlies. In these cases, greenhouse forcing stabilizes at a much lower level
296 and stratospheric ozone forcing can largely compensate the increase in greenhouse gases.

297

298 Projected 21st Century trends from CMIP6 models in the latitude of the maximum westerlies
299 also show large regional differences, with the strongest poleward trends over the Atlantic
300 and east Pacific Oceans, and somewhat weaker poleward trends in the Indian Ocean (Fig.
301 3b). Both CMIP5 and CMIP6 show similar regional patterns in the MMM trends in the
302 meridional location of the westerlies (with a spatial correlation, $R=0.83$). However, CMIP6
303 MMM trends in the meridional location are weaker as compared to CMIP5 MMM trends
304 (Fig. 3b). The weaker poleward shift in CMIP6 MMM as compared to CMIP5 MMM is
305 consistent with the reduction in the equatorward bias in the meridional location of
306 westerlies in CMIP6 MMM as compared to CMIP5 MMM, as models with a larger
307 equatorward bias also tend to show a larger projected poleward shift (Bracegirdle et al.,

308 2013). Significant projected trends in the strength of westerlies under the SSP585 scenario
309 of CMIP6 are evident at all longitudes, with stronger trends centered south of Australia and
310 within the Drake Passage (Fig. 3c). Again, consistent regional patterns are found between
311 both the model generations ($R=0.9$, Fig. 3c). However, the projected 21st Century trends are
312 stronger in the CMIP5 MMM as compared to CMIP6 MMM in all regions except for the
313 Atlantic (Fig. 3c).

314

315 **5. Summary and Discussion**

316 In the past a wide range of wind shifts and accelerations have been used to force ocean
317 models in order to examine the response of the Southern Ocean and the Antarctic margin to
318 past and projected changes in SH westerlies. Understanding future changes has also been
319 hampered by the fact that CMIP5 models showed a significant equatorward bias in the
320 location of the SH westerlies. Previous work has shown that projected wind changes are
321 sensitive to the model's mean state. In particular, models with larger equatorward biases
322 tend to show larger projected poleward wind shifts (Bracegirdle et al., 2013). As such, an
323 anomalous wind shift based on a climate model projection (or from an ensemble of models)
324 will retain a signature of the model's mean state bias (e.g. Duran et al., 2020).

325

326 In this study we found a significant reduction in the equatorward bias in the location of SH
327 westerlies in CMIP6 models as compared to CMIP5 models, with the location of maximum
328 surface westerlies in closer agreement with the position of maximum surface westerlies in
329 the ERA5 reanalysis. Given the sensitivity of model projections to mean state biases, CMIP6
330 models thus likely offer a more credible estimate of past and future changes in SH
331 westerlies for forcing ocean model simulations. We also found that the reanalysis time

332 period (41 years from 1979-2019) is too short to provide an estimate of the forced trends in
333 the SH westerlies, as the trends over this multi-decadal period appear to be strongly
334 influenced by internal climate variability (see also Schneider et al., 2015; D. Yang et al.,
335 2020). Moreover, it is likely that any anthropogenic forced component of regional or
336 seasonal differences in the reanalysis trends is dominated by internal variability. MMM
337 regional and seasonal trend patterns in both the latitude and strength of the maximum
338 winds only become consistent between CMIP5 and CMIP6 when considering centennial
339 time-scale trends.

340

341 Based on the discussion above, we can provide a set of recommendations for forcing ocean
342 model simulations with past and projected changes in SH surface winds: 1) Recent observed
343 wind trends over the Southern Ocean likely include a substantial component of internal
344 decadal variability, and thus should not be assumed to be indicative of forced changes
345 alone. 2) CMIP6 models should be used instead of CMIP5 models for guiding the forcing
346 used in ocean model simulations, for both past and future changes in the SH westerlies,
347 given the much reduced mean state biases. 3) Seasonal variations in trends in both the
348 location and the strength of the westerlies should be considered for simulations where
349 seasonal changes are important (e.g., for studies examining seasonal changes in mode water
350 formation, or Antarctic sea ice variability). 4) As ocean circulation is sensitive to the position
351 of the wind maximum/wind stress curl, prescribed wind forcing should also include regional
352 variations in surface wind trends. This is particularly relevant for projections where regional
353 differences in trends can be as large as 150% for the location and 90% for the strength of
354 the westerlies (Fig. 3b,3c).

355

356 While we have focused on ensemble average hindcasts and projections for CMIP5 and
357 CMIP6 simulations, using the multi-model mean to construct zonal-mean wind forcing
358 anomalies presents some problems. For example, only prescribing a zonal wind anomaly is
359 not dynamically consistent if no changes are made to the meridional winds. In addition, the
360 application of a zonal wind perturbation to daily reanalysis fields will distort the geometry of
361 storms. Tapering regions by applying wind anomalies over a particular latitude band in the
362 SH extratropics can also create spurious wind stress curl anomalies (e.g. Maher et al., 2018).
363 One option to minimize these limitations is to use output from individual models as
364 boundary forcing (e.g. Naughten et al., 2018), something commonly done for atmospheric
365 downscaling projects (e.g. Evans et al., 2014) . This is a more viable option now that CMIP6
366 models have minimal equatorward bias in the SH westerlies as compared to CMIP5. Using
367 multiple models would also provide a means to estimate uncertainty in the projections.

368

369 Under a high emission scenario, a poleward intensification of the SH surface westerlies is
370 projected to continue in the future despite the projected recovery of stratospheric ozone,
371 because greenhouse gas forcing dominates the future trends across all seasons. We have
372 provided quantitative information on the past and projected future changes in zonal mean
373 position and strength of the surface westerlies over both annual and seasonal time scales
374 (Table S3). This can be used to guide the forcing of idealized ocean model simulations with
375 zonally averaged past and future changes in the SH westerlies.

376

377 **Data Availability Statements**

378 The datasets analyzed in this study are all publicly available. Data for CMIP5 and CMIP6
379 models can be obtained from the Earth Systems Grid Federation website

380 (CMIP5-<https://esgf-node.llnl.gov/projects/cmip5/> and CMIP6- [https://esgf-
382 node.llnl.gov/projects/cmip6/](https://esgf-
381 node.llnl.gov/projects/cmip6/)). ERA5 data can be downloaded from ECMWF website
(<https://www.ecmwf.int/en/forecasts/datasets/reanalysis-datasets/era5>).

383

384 **Acknowledgements**

385 This study was supported by the Australian Research Council (grants
386 CE170100023, FL150100035). R.G. is supported by the Scientia PhD scholarship from the
387 University of New South Wales. M.H.E. is also supported by the Earth Science and Climate
388 Change Hub of the Australian Government's National Environmental Science Programme
389 (NESP) and the Centre for Southern Hemisphere Oceans Research (CSHOR), a joint research
390 centre between QNLM, CSIRO, UNSW and UTAS. Analysis were conducted on the National
391 Computational Infrastructure (NCI) facility based in Canberra, Australia.

392

393

394

395

396 **References**

397 Arblaster, J. M., & Meehl, G. A. (2006). Contributions of External Forcings to Southern
398 Annular Mode Trends. *Journal of Climate*, *19*(12), 2896–2905.

399 <https://doi.org/10.1175/JCLI3774.1>

400 Austin, J., & Wilson, R. J. (2006). Ensemble simulations of the decline and recovery of
401 stratospheric ozone. *Journal of Geophysical Research: Atmospheres*, *111*(D16).

402 <https://doi.org/10.1029/2005JD006907>

403 Bauer, S. E., Tsigaridis, K., Faluvegi, G., Kelley, M., Lo, K. K., Miller, R. L., et al. (2020).

404 Historical (1850-2014) aerosol evolution and role on climate forcing using the GISS
405 ModelE2.1 contribution to CMIP6. *Journal of Advances in Modeling Earth Systems*,
406 e2019MS001978. <https://doi.org/10.1029/2019MS001978>

407 Boucher, O., Servonnat, J., Albright, A. L., Aumont, O., Balkanski, Y., Bastrikov, V., et al.
408 (2020). Presentation and evaluation of the IPSL-CM6A-LR climate model. *Journal of*
409 *Advances in Modeling Earth Systems*, e2019MS002010.
410 <https://doi.org/10.1029/2019MS002010>

411 Bracegirdle, T J, Holmes, C. R., Hosking, J. S., Marshall, G. J., Osman, M., Patterson, M., &
412 Rackow, T. (2020). Improvements in Circumpolar Southern Hemisphere Extratropical
413 Atmospheric Circulation in CMIP6 Compared to CMIP5. *Earth and Space Science*, 7(6),
414 e2019EA001065. <https://doi.org/10.1029/2019EA001065>

415 Bracegirdle, Thomas J. (2013). Climatology and recent increase of westerly winds over the
416 Amundsen Sea derived from six reanalyses. *International Journal of Climatology*, 33(4),
417 843–851. <https://doi.org/10.1002/joc.3473>

418 Bracegirdle, Thomas J., Shuckburgh, E., Sallee, J.-B., Wang, Z., Meijers, A. J. S., Bruneau, N.,
419 et al. (2013). Assessment of surface winds over the Atlantic, Indian, and Pacific Ocean
420 sectors of the Southern Ocean in CMIP5 models: historical bias, forcing response, and
421 state dependence. *Journal of Geophysical Research: Atmospheres*, 118(2), 547–562.
422 <https://doi.org/10.1002/jgrd.50153>

423 Cao, J., Wang, B., Yang, Y.-M., Ma, L., Li, J., Sun, B., et al. (2018). The NUIST Earth System
424 Model (NESM) version 3: description and preliminary evaluation. *Geosci. Model Dev.*,
425 11(7), 2975–2993. <https://doi.org/10.5194/gmd-11-2975-2018>

426 Cariolle, D., & Teyssèdre, H. (2007). A revised linear ozone photochemistry parameterization
427 for use in transport and general circulation models: multi-annual simulations. *Atmos.*

428 *Chem. Phys.*, 7(9), 2183–2196. <https://doi.org/10.5194/acp-7-2183-2007>

429 Ceppi, P., Hwang, Y.-T., Frierson, D. M. W., & Hartmann, D. L. (2012). Southern Hemisphere
430 jet latitude biases in CMIP5 models linked to shortwave cloud forcing. *Geophysical*
431 *Research Letters*, 39(19). <https://doi.org/10.1029/2012GL053115>

432 Cionni, I., Eyring, V., Lamarque, J. F., Randel, W. J., Stevenson, D. S., Wu, F., et al. (2011).
433 Ozone database in support of CMIP5 simulations: Results and corresponding radiative
434 forcing. *Atmospheric Chemistry and Physics*, 11(21), 11267–11292.
435 <https://doi.org/10.5194/acp-11-11267-2011>

436 Collins, W. J., Bellouin, N., Doutriaux-Boucher, M., Gedney, N., Halloran, P., Hinton, T., et al.
437 (2011). Development and evaluation of an Earth-System model – HadGEM2. *Geosci.*
438 *Model Dev.*, 4(4), 1051–1075. <https://doi.org/10.5194/gmd-4-1051-2011>

439 Delworth, T. L., & Zeng, F. (2008). Simulated impact of altered Southern Hemisphere winds
440 on the Atlantic Meridional Overturning Circulation. *Geophysical Research Letters*,
441 35(20), L20708. <https://doi.org/10.1029/2008GL035166>

442 Dix, M., Vohralik, P., Bi, D., Rashid, H., Marsland, S., O’Farrell, S., et al. (2013). The ACCESS
443 coupled model: Documentation of core CMIP5 simulations and initial results. *Australian*
444 *Meteorological and Oceanographic Journal*, 63(1), 83–99.
445 <https://doi.org/10.22499/2.6301.006>

446 Donner, L. J., Wyman, B. L., Hemler, R. S., Horowitz, L. W., Ming, Y., Zhao, M., et al. (2011).
447 The Dynamical Core, Physical Parameterizations, and Basic Simulation Characteristics of
448 the Atmospheric Component AM3 of the GFDL Global Coupled Model CM3. *Journal of*
449 *Climate*, 24(13), 3484–3519. <https://doi.org/10.1175/2011JCLI3955.1>

450 Downes, S. M., Langlais, C., Brook, J. P., & Spence, P. (2017). Regional Impacts of the
451 Westerly Winds on Southern Ocean Mode and Intermediate Water Subduction. *Journal*

452 *of Physical Oceanography*, 47(10), 2521–2530. <https://doi.org/10.1175/JPO-D-17->
453 0106.1

454 Dufresne, J.-L., Foujols, M.-A., Denvil, S., Caubel, A., Marti, O., Aumont, O., et al. (2013).
455 Climate change projections using the IPSL-CM5 Earth System Model: from CMIP3 to
456 CMIP5. *Climate Dynamics*, 40(9), 2123–2165. <https://doi.org/10.1007/s00382-012->
457 1636-1

458 Dunne, J. P., John, J. G., Adcroft, A. J., Griffies, S. M., Hallberg, R. W., Shevliakova, E., et al.
459 (2012). GFDL's ESM2 Global Coupled Climate–Carbon Earth System Models. Part I:
460 Physical Formulation and Baseline Simulation Characteristics. *Journal of Climate*,
461 25(19), 6646–6665. <https://doi.org/10.1175/JCLI-D-11-00560.1>

462 Duran, E. R., England, M. H., & Spence, P. (2020). Surface Ocean Warming Around Australia
463 Driven by Interannual Variability and Long-Term Trends in Southern Hemisphere
464 Westerlies. *Geophysical Research Letters*, 47(9), e2019GL086605.
465 <https://doi.org/10.1029/2019GL086605>

466 Evans, J. P., Ji, F., Lee, C., Smith, P., Argüeso, D., & Fita, L. (2014). Design of a regional
467 climate modelling projection ensemble experiment - NARClIM. *Geoscientific Model*
468 *Development*. <https://doi.org/10.5194/gmd-7-621-2014>

469 Eyring, V., Cionni, I., Bodeker, G. E., Charlton-Perez, A. J., Kinnison, D. E., Scinocca, J. F., et al.
470 (2010). Multi-model assessment of stratospheric ozone return dates and ozone
471 recovery in CCMVal-2 models. *Atmospheric Chemistry and Physics*, 10(19), 9451–9472.
472 <https://doi.org/10.5194/acp-10-9451-2010>

473 Frankcombe, L. M., Spence, P., Hogg, A. M., England, M. H., & Griffies, S. M. (2013). Sea level
474 changes forced by Southern Ocean winds. *Geophysical Research Letters*, 40(21), 5710–
475 5715. <https://doi.org/10.1002/2013GL058104>

476 Giorgetta, M. A., Jungclaus, J., Reick, C. H., Legutke, S., Bader, J., Böttinger, M., et al. (2013).
477 Climate and carbon cycle changes from 1850 to 2100 in MPI-ESM simulations for the
478 Coupled Model Intercomparison Project phase 5. *Journal of Advances in Modeling*
479 *Earth Systems*, 5(3), 572–597. <https://doi.org/10.1002/jame.20038>

480 Gordon, C., Cooper, C., Senior, C. A., Banks, H., Gregory, J. M., Johns, T. C., et al. (2000). The
481 simulation of SST, sea ice extents and ocean heat transports in a version of the Hadley
482 Centre coupled model without flux adjustments. *Climate Dynamics*, 16(2), 147–168.
483 <https://doi.org/10.1007/s003820050010>

484 Goyal, R., England, M. H., Sen Gupta, A., & Jucker, M. (2019). Reduction in surface climate
485 change achieved by the 1987 Montreal Protocol. *Environmental Research Letters*,
486 14(12), 124041. <https://doi.org/10.1088/1748-9326/ab4874>

487 Gutjahr, O., Putrasahan, D., Lohmann, K., Jungclaus, J. H., von Storch, J.-S., Brüggemann, N.,
488 et al. (2019). Max Planck Institute Earth System Model (MPI-ESM1.2) for the High-
489 Resolution Model Intercomparison Project (HighResMIP). *Geosci. Model Dev.*, 12(7),
490 3241–3281. <https://doi.org/10.5194/gmd-12-3241-2019>

491 Hall, A., & Visbeck, M. (2002). Synchronous Variability in the Southern Hemisphere
492 Atmosphere, Sea Ice, and Ocean Resulting from the Annular Mode*. *Journal of Climate*,
493 15(21), 3043–3057. [https://doi.org/10.1175/1520-0442\(2002\)015<3043:SVITSH>2.0.CO;2](https://doi.org/10.1175/1520-0442(2002)015<3043:SVITSH>2.0.CO;2)

495 Hansen, J., Sato, M., Ruedy, R., Kharecha, P., Lacis, A., Miller, R., et al. (2007). Climate
496 simulations for 1880–2003 with GISS modelE. *Climate Dynamics*, 29(7), 661–696.
497 <https://doi.org/10.1007/s00382-007-0255-8>

498 He, B., Bao, Q., Wang, X., Zhou, L., Wu, X., Liu, Y., et al. (2019). CAS FGOALS-f3-L Model
499 Datasets for CMIP6 Historical Atmospheric Model Intercomparison Project Simulation.

500 *Advances in Atmospheric Sciences*, 36(8), 771–778. <https://doi.org/10.1007/s00376->
501 019-9027-8

502 Held, I. M., Guo, H., Adcroft, A., Dunne, J. P., Horowitz, L. W., Krasting, J., et al. (2019).
503 Structure and Performance of GFDL’s CM4.0 Climate Model. *Journal of Advances in*
504 *Modeling Earth Systems*, 11(11), 3691–3727. <https://doi.org/10.1029/2019MS001829>

505 Hersbach, H., Bell, B., Berrisford, P., Hirahara, S., Horányi, A., Muñoz-Sabater, J., et al.
506 (2020). The ERA5 global reanalysis. *Quarterly Journal of the Royal Meteorological*
507 *Society*, qj.3803. <https://doi.org/10.1002/qj.3803>

508 Hogg, A. M., Spence, P., Saenko, O. A., & Downes, S. M. (2017). The Energetics of Southern
509 Ocean Upwelling. *Journal of Physical Oceanography*, 47(1), 135–153.
510 <https://doi.org/10.1175/JPO-D-16-0176.1>

511 Holland, P. R., Bracegirdle, T. J., Dutrieux, P., Jenkins, A., & Steig, E. J. (2019). West Antarctic
512 ice loss influenced by internal climate variability and anthropogenic forcing. *Nature*
513 *Geoscience*, 12(9), 718–724. <https://doi.org/10.1038/s41561-019-0420-9>

514 Horowitz, L. W., Walters, S., Mauzerall, D. L., Emmons, L. K., Rasch, P. J., Granier, C., et al.
515 (2003). A global simulation of tropospheric ozone and related tracers: Description and
516 evaluation of MOZART, version 2. *Journal of Geophysical Research: Atmospheres*,
517 108(D24). <https://doi.org/10.1029/2002JD002853>

518 Iversen, T., Bentsen, M., Bethke, I., Debernard, J. B., Kirkevåg, A., Seland, Ø., et al. (2013).
519 The Norwegian Earth System Model, NorESM1-M – Part 2: Climate response and
520 scenario projections. *Geosci. Model Dev.*, 6(2), 389–415. <https://doi.org/10.5194/gmd->
521 6-389-2013

522 Jones, C. D., Hughes, J. K., Bellouin, N., Hardiman, S. C., Jones, G. S., Knight, J., et al. (2011).
523 The HadGEM2-ES implementation of CMIP5 centennial simulations. *Geosci. Model*

524 *Dev.*, 4(3), 543–570. <https://doi.org/10.5194/gmd-4-543-2011>

525 Kalnay, E., Kanamitsu, M., Kistler, R., Collins, W., Deaven, D., Gandin, L., et al. (1996). The
526 NCEP/NCAR 40-Year Reanalysis Project. *Bulletin of the American Meteorological*
527 *Society*, 77(3), 437–472. [https://doi.org/10.1175/1520-](https://doi.org/10.1175/1520-0477(1996)077<0437:TNYRP>2.0.CO;2)
528 [0477\(1996\)077<0437:TNYRP>2.0.CO;2](https://doi.org/10.1175/1520-0477(1996)077<0437:TNYRP>2.0.CO;2)

529 Kawase, H., Nagashima, T., Sudo, K., & Nozawa, T. (2011). Future changes in tropospheric
530 ozone under Representative Concentration Pathways (RCPs). *Geophysical Research*
531 *Letters*, 38(5). <https://doi.org/10.1029/2010GL046402>

532 Kobayashi, S., OTA, Y., HARADA, Y., EBITA, A., MORIYA, M., ONODA, H., et al. (2015). The
533 JRA-55 Reanalysis: General Specifications and Basic Characteristics. *Journal of the*
534 *Meteorological Society of Japan. Ser. II*, 93(1), 5–48. [https://doi.org/10.2151/jmsj.2015-](https://doi.org/10.2151/jmsj.2015-001)
535 [001](https://doi.org/10.2151/jmsj.2015-001)

536 Krasting, J. P., John, J. G., Blanton, C., McHugh, C., Nikonov, S., Radhakrishnan, A., et al.
537 (2018). NOAA-GFDL GFDL-ESM4 model output prepared for CMIP6 CMIP historical.
538 Earth System Grid Federation. <https://doi.org/10.22033/ESGF/CMIP6.8597>

539 Lamarque, J.-F., Bond, T. C., Eyring, V., Granier, C., Heil, A., Klimont, Z., et al. (2010).
540 Historical (1850–2000) gridded anthropogenic and biomass burning emissions of
541 reactive gases and aerosols: methodology and application. *Atmos. Chem. Phys.*, 10(15),
542 7017–7039. <https://doi.org/10.5194/acp-10-7017-2010>

543 Lamarque, J.-F., Emmons, L. K., Hess, P. G., Kinnison, D. E., Tilmes, S., Vitt, F., et al. (2012).
544 CAM-chem: description and evaluation of interactive atmospheric chemistry in the
545 Community Earth System Model. *Geosci. Model Dev.*, 5(2), 369–411.
546 <https://doi.org/10.5194/gmd-5-369-2012>

547 Le Quere, C., Rodenbeck, C., Buitenhuis, E. T., Conway, T. J., Langenfelds, R., Gomez, A., et

548 al. (2007). Saturation of the Southern Ocean CO₂ Sink Due to Recent Climate Change.
549 *Science*, 316(5832), 1735–1738. <https://doi.org/10.1126/science.1136188>

550 Lee, J., Kim, J., Sun, M.-A., Kim, B.-H., Moon, H., Sung, H. M., et al. (2020). Evaluation of the
551 Korea Meteorological Administration Advanced Community Earth-System model (K-
552 ACE). *Asia-Pacific Journal of Atmospheric Sciences*, 56(3), 381–395.
553 <https://doi.org/10.1007/s13143-019-00144-7>

554 Li, F., Orsolini, Y. J., Keenlyside, N., Shen, M.-L., Counillon, F., & Wang, Y. G. (2019). Impact of
555 Snow Initialization in Subseasonal-to-Seasonal Winter Forecasts With the Norwegian
556 Climate Prediction Model. *Journal of Geophysical Research: Atmospheres*, 124(17–18),
557 10033–10048. <https://doi.org/10.1029/2019JD030903>

558 Lovenduski, N. S., Gruber, N., Doney, S. C., & Lima, I. D. (2007). Enhanced CO₂ outgassing in
559 the Southern Ocean from a positive phase of the Southern Annular Mode. *Global*
560 *Biogeochemical Cycles*, 21(2). <https://doi.org/10.1029/2006GB002900>

561 Maher, N., England, M. H., Gupta, A. Sen, & Spence, P. (2018). Role of Pacific trade winds in
562 driving ocean temperatures during the recent slowdown and projections under a wind
563 trend reversal. *Climate Dynamics*. <https://doi.org/10.1007/s00382-017-3923-3>

564 Marshall, G. J. (2003). Trends in the Southern Annular Mode from Observations and
565 Reanalyses. *Journal of Climate*, 16(24), 4134–4143. [https://doi.org/10.1175/1520-0442\(2003\)016<4134:TITSAM>2.0.CO;2](https://doi.org/10.1175/1520-0442(2003)016<4134:TITSAM>2.0.CO;2)

567 Martin, G. M., Bellouin, N., Collins, W. J., Culverwell, I. D., Halloran, P. R., Hardiman, S. C., et
568 al. (2011). The HadGEM2 family of Met Office Unified Model climate configurations.
569 *Geoscientific Model Development*, 4(3), 723–757. [https://doi.org/10.5194/gmd-4-723-](https://doi.org/10.5194/gmd-4-723-2011)
570 2011

571 Mauritsen, T., Bader, J., Becker, T., Behrens, J., Bittner, M., Brokopf, R., et al. (2019).

572 Developments in the MPI-M Earth System Model version 1.2 (MPI-ESM1.2) and Its
573 Response to Increasing CO₂. *Journal of Advances in Modeling Earth Systems*, 11(4),
574 998–1038. <https://doi.org/10.1029/2018MS001400>

575 Naughten, K. A., Meissner, K. J., Galton-Fenzi, B. K., England, M. H., Timmermann, R., &
576 Hellmer, H. H. (2018). Future Projections of Antarctic Ice Shelf Melting Based on CMIP5
577 Scenarios. *Journal of Climate*, 31(13), 5243–5261. [https://doi.org/10.1175/JCLI-D-17-](https://doi.org/10.1175/JCLI-D-17-0854.1)
578 0854.1

579 Newman, P. A., Nash, E. R., Kawa, S. R., Montzka, S. A., & Schauffler, S. M. (2006). When will
580 the Antarctic ozone hole recover? *Geophysical Research Letters*, 33(12), 1–5.
581 <https://doi.org/10.1029/2005GL025232>

582 O'Connor, F. M., Johnson, C. E., Morgenstern, O., Abraham, N. L., Braesicke, P., Dalvi, M., et
583 al. (2014). Evaluation of the new UKCA climate-composition model – Part 2: The
584 Troposphere. *Geosci. Model Dev.*, 7(1), 41–91. <https://doi.org/10.5194/gmd-7-41-2014>

585 O'Neill, B. C., Tebaldi, C., van Vuuren, D. P., Eyring, V., Friedlingstein, P., Hurtt, G., et al.
586 (2016). The Scenario Model Intercomparison Project (ScenarioMIP) for CMIP6.
587 *Geoscientific Model Development*, 9(9), 3461–3482. [https://doi.org/10.5194/gmd-9-](https://doi.org/10.5194/gmd-9-3461-2016)
588 3461-2016

589 Oke, P. R., & England, M. H. (2004). Oceanic Response to Changes in the Latitude of the
590 Southern Hemisphere Subpolar Westerly Winds. *Journal of Climate*, 17(5), 1040–1054.
591 [https://doi.org/10.1175/1520-0442\(2004\)017<1040:ORTCIT>2.0.CO;2](https://doi.org/10.1175/1520-0442(2004)017<1040:ORTCIT>2.0.CO;2)

592 Rong, X., Li, J., Chen, H., Xin, Y., Su, J., Hua, L., et al. (2018). The CAMS Climate System Model
593 and a Basic Evaluation of Its Climatology and Climate Variability Simulation. *Journal of*
594 *Meteorological Research*, 32(6), 839–861. <https://doi.org/10.1007/s13351-018-8058-x>

595 Roscoe, H. K., & Haigh, J. D. (2007). Influences of ozone depletion, the solar cycle and the

596 QBO on the Southern Annular Mode. *Quarterly Journal of the Royal Meteorological*
597 *Society*, 133(628), 1855–1864. <https://doi.org/10.1002/qj.153>

598 Rotstayn, L. D., Jeffrey, S. J., Collier, M. A., Dravitzki, S. M., Hirst, A. C., Syktus, J. I., & Wong,
599 K. K. (2012). Aerosol- and greenhouse gas-induced changes in summer rainfall and
600 circulation in the Australasian region: a study using single-forcing climate simulations.
601 *Atmos. Chem. Phys.*, 12(14), 6377–6404. <https://doi.org/10.5194/acp-12-6377-2012>

602 Schmidt, G. A., Ruedy, R., Hansen, J. E., Aleinov, I., Bell, N., Bauer, M., et al. (2006). Present-
603 Day Atmospheric Simulations Using GISS ModelE: Comparison to In Situ, Satellite, and
604 Reanalysis Data. *Journal of Climate*, 19(2), 153–192.
605 <https://doi.org/10.1175/JCLI3612.1>

606 Schneider, D. P., Deser, C., & Fan, T. (2015). Comparing the Impacts of Tropical SST
607 Variability and Polar Stratospheric Ozone Loss on the Southern Ocean Westerly Winds.
608 *Journal of Climate*, 28(23), 9350–9372. <https://doi.org/10.1175/JCLI-D-15-0090.1>

609 Séférian, R., Nabat, P., Michou, M., Saint-Martin, D., Voldoire, A., Colin, J., et al. (2019).
610 Evaluation of CNRM Earth System Model, CNRM-ESM2-1: Role of Earth System
611 Processes in Present-Day and Future Climate. *Journal of Advances in Modeling Earth*
612 *Systems*, 11(12), 4182–4227. <https://doi.org/10.1029/2019MS001791>

613 Sellar, A. A., Jones, C. G., Mulcahy, J. P., Tang, Y., Yool, A., Wiltshire, A., et al. (2019).
614 UKESM1: Description and Evaluation of the U.K. Earth System Model. *Journal of*
615 *Advances in Modeling Earth Systems*, 11(12), 4513–4558.
616 <https://doi.org/10.1029/2019MS001739>

617 Semmler, A.-T., Danilov, S., Gierz, P., Goessling, H., Hegewald, J., Hinrichs, C., et al. (2020).
618 Simulations for CMIP6 with the AWI climate model AWI-CM-1-1. *Earth and Space*
619 *Science Open Archive*. <https://doi.org/10.1002/essoar.10501538.1>

620 Sen Gupta, A., & England, M. H. (2006). Coupled Ocean–Atmosphere–Ice Response to
621 Variations in the Southern Annular Mode. *Journal of Climate*, *19*(18), 4457–4486.
622 <https://doi.org/10.1175/JCLI3843.1>

623 Shindell, D T, Pechony, O., Voulgarakis, A., Faluvegi, G., Nazarenko, L., Lamarque, J.-F., et al.
624 (2013). Interactive ozone and methane chemistry in GISS-E2 historical and future
625 climate simulations. *Atmos. Chem. Phys.*, *13*(5), 2653–2689.
626 <https://doi.org/10.5194/acp-13-2653-2013>

627 Shindell, Drew T. (2004). Southern Hemisphere climate response to ozone changes and
628 greenhouse gas increases. *Geophysical Research Letters*, *31*(18), L18209.
629 <https://doi.org/10.1029/2004GL020724>

630 Spence, P., Griffies, S. M., England, M. H., Hogg, A. M., Saenko, O. A., & Jourdain, N. C.
631 (2014). Rapid subsurface warming and circulation changes of Antarctic coastal waters
632 by poleward shifting winds. *Geophysical Research Letters*, *41*(13), 4601–4610.
633 <https://doi.org/10.1002/2014GL060613>

634 Stouffer, R. (2019). U of Arizona MCM-UA-1-0 model output prepared for CMIP6 CMIP
635 historical. Earth System Grid Federation. <https://doi.org/10.22033/ESGF/CMIP6.2421>

636 Swart, N. C., Cole, J. N. S., Kharin, V. V., Lazare, M., Scinocca, J. F., Gillett, N. P., et al. (2019).
637 The Canadian Earth System Model version 5 (CanESM5.0.3). *Geosci. Model Dev.*,
638 *12*(11), 4823–4873. <https://doi.org/10.5194/gmd-12-4823-2019>

639 Szopa, S., Balkanski, Y., Schulz, M., Bekki, S., Cugnet, D., Fortems-Cheiney, A., et al. (2013).
640 Aerosol and ozone changes as forcing for climate evolution between 1850 and 2100.
641 *Climate Dynamics*, *40*(9), 2223–2250. <https://doi.org/10.1007/s00382-012-1408-y>

642 Tatebe, H., Ogura, T., Nitta, T., Komuro, Y., Ogochi, K., Takemura, T., et al. (2019).
643 Description and basic evaluation of simulated mean state, internal variability, and

644 climate sensitivity in MIROC6. *Geosci. Model Dev.*, 12(7), 2727–2765.
645 <https://doi.org/10.5194/gmd-12-2727-2019>

646 Thompson, D. W. J. (2002). Interpretation of Recent Southern Hemisphere Climate Change.
647 *Science*, 296(5569), 895–899. <https://doi.org/10.1126/science.1069270>

648 Thompson, D. W. J., Solomon, S., Kushner, P. J., England, M. H., Grise, K. M., & Karoly, D. J.
649 (2011). Signatures of the Antarctic ozone hole in Southern Hemisphere surface climate
650 change. *Nature Geoscience*, 4(11), 741–749. <https://doi.org/10.1038/ngeo1296>

651 Toggweiler, J. R., Russell, J. L., & Carson, S. R. (2006). Midlatitude westerlies, atmospheric
652 CO₂, and climate change during the ice ages. *Paleoceanography*, 21(2).
653 <https://doi.org/10.1029/2005PA001154>

654 Vichi, M., Navarra, A., & Fogli, P. G. (2013). Adjustment of the natural ocean carbon cycle to
655 negative emission rates. *Climatic Change*, 118(1), 105–118.
656 <https://doi.org/10.1007/s10584-012-0677-0>

657 Voldoire, A., Sanchez-Gomez, E., Salas y Mélia, D., Decharme, B., Cassou, C., Sénési, S., et al.
658 (2013). The CNRM-CM5.1 global climate model: description and basic evaluation.
659 *Climate Dynamics*, 40(9), 2091–2121. <https://doi.org/10.1007/s00382-011-1259-y>

660 Voldoire, A., Saint-Martin, D., Sénési, S., Decharme, B., Alias, A., Chevallier, M., et al. (2019).
661 Evaluation of CMIP6 DECK Experiments With CNRM-CM6-1. *Journal of Advances in*
662 *Modeling Earth Systems*, 11(7), 2177–2213. <https://doi.org/10.1029/2019MS001683>

663 Volodin, E., & Gritsun, A. (2018). Simulation of observed climate changes in 1850-2014 with
664 climate model INM-CM5. *Earth System Dynamics*, 9(4), 1235–1242.
665 <https://doi.org/10.5194/esd-9-1235-2018>

666 Volodin, E M, Dianskii, N. A., & Gusev, A. V. (2010). Simulating present-day climate with the
667 INMCM4.0 coupled model of the atmospheric and oceanic general circulations.

668 *Izvestiya, Atmospheric and Oceanic Physics*, 46(4), 414–431.
669 <https://doi.org/10.1134/S000143381004002X>

670 Volodin, Evgenii M, Mortikov, E. V, Kostykin, S. V, Galin, V. Y., Lykossov, V. N., Gritsun, A. S.,
671 et al. (2018). Simulation of the modern climate using the INM-CM48 climate model.
672 *Russian Journal of Numerical Analysis and Mathematical Modelling*, 33(6), 367–374.
673 <https://doi.org/https://doi.org/10.1515/rnam-2018-0032>

674 von Salzen, K., Scinocca, J. F., McFarlane, N. A., Li, J., Cole, J. N. S., Plummer, D., et al. (2013).
675 The Canadian Fourth Generation Atmospheric Global Climate Model (CanAM4). Part I:
676 Representation of Physical Processes. *Atmosphere-Ocean*, 51(1), 104–125.
677 <https://doi.org/10.1080/07055900.2012.755610>

678 Watanabe, S., Hajima, T., Sudo, K., Nagashima, T., Takemura, T., Okajima, H., et al. (2011).
679 MIROC-ESM 2010: model description and basic results of CMIP5-20c3m experiments.
680 *Geosci. Model Dev.*, 4(4), 845–872. <https://doi.org/10.5194/gmd-4-845-2011>

681 Waugh, D. W., Primeau, F., DeVries, T., & Holzer, M. (2013). Recent Changes in the
682 Ventilation of the Southern Oceans. *Science*, 339(6119), 568–570.
683 <https://doi.org/10.1126/science.1225411>

684 Waugh, D. W., McC. Hogg, A., Spence, P., England, M. H., & Haine, T. W. N. (2019). Response
685 of Southern Ocean Ventilation to Changes in Midlatitude Westerly Winds. *Journal of*
686 *Climate*, 32(17), 5345–5361. <https://doi.org/10.1175/JCLI-D-19-0039.1>

687 Waugh, D. W., Banerjee, A., Fyfe, J. C., & Polvani, L. M. (2020). Contrasting recent trends in
688 Southern Hemisphere Westerlies across different ocean basins. *Earth and Space*
689 *Science Open Archive*. <https://doi.org/10.1002/essoar.10503156.1>

690 Wu, T., Lu, Y., Fang, Y., Xin, X., Li, L., Li, W., et al. (2019). The Beijing Climate Center Climate
691 System Model (BCC-CSM): The main progress from CMIP5 to CMIP6. *Geoscientific*

692 *Model Development*, 12(4), 1573–1600. <https://doi.org/10.5194/gmd-12-1573-2019>

693 Wu, T., Zhang, F., Zhang, J., Jie, W., Zhang, Y., Wu, F., et al. (2020). Beijing Climate Center
694 Earth System Model version 1 (BCC-ESM1): Model description and evaluation of
695 aerosol simulations. *Geoscientific Model Development*, 13(3), 977–1005.
696 <https://doi.org/10.5194/gmd-13-977-2020>

697 Yang, D., Arblaster, J. M., Meehl, G. A., England, M. H., Lim, E.-P., Bates, S., & Rosenbloom,
698 N. (2020). Role of Tropical Variability in Driving Decadal Shifts in the Southern
699 Hemisphere Summertime Eddy-Driven Jet. *Journal of Climate*, 33(13), 5445–5463.
700 <https://doi.org/10.1175/JCLI-D-19-0604.1>

701 Yang, H., Lohmann, G., Wei, W., Dima, M., Ionita, M., & Liu, J. (2016). Intensification and
702 poleward shift of subtropical western boundary currents in a warming climate. *Journal*
703 *of Geophysical Research: Oceans*, 121(7), 4928–4945.
704 <https://doi.org/10.1002/2015JC011513>

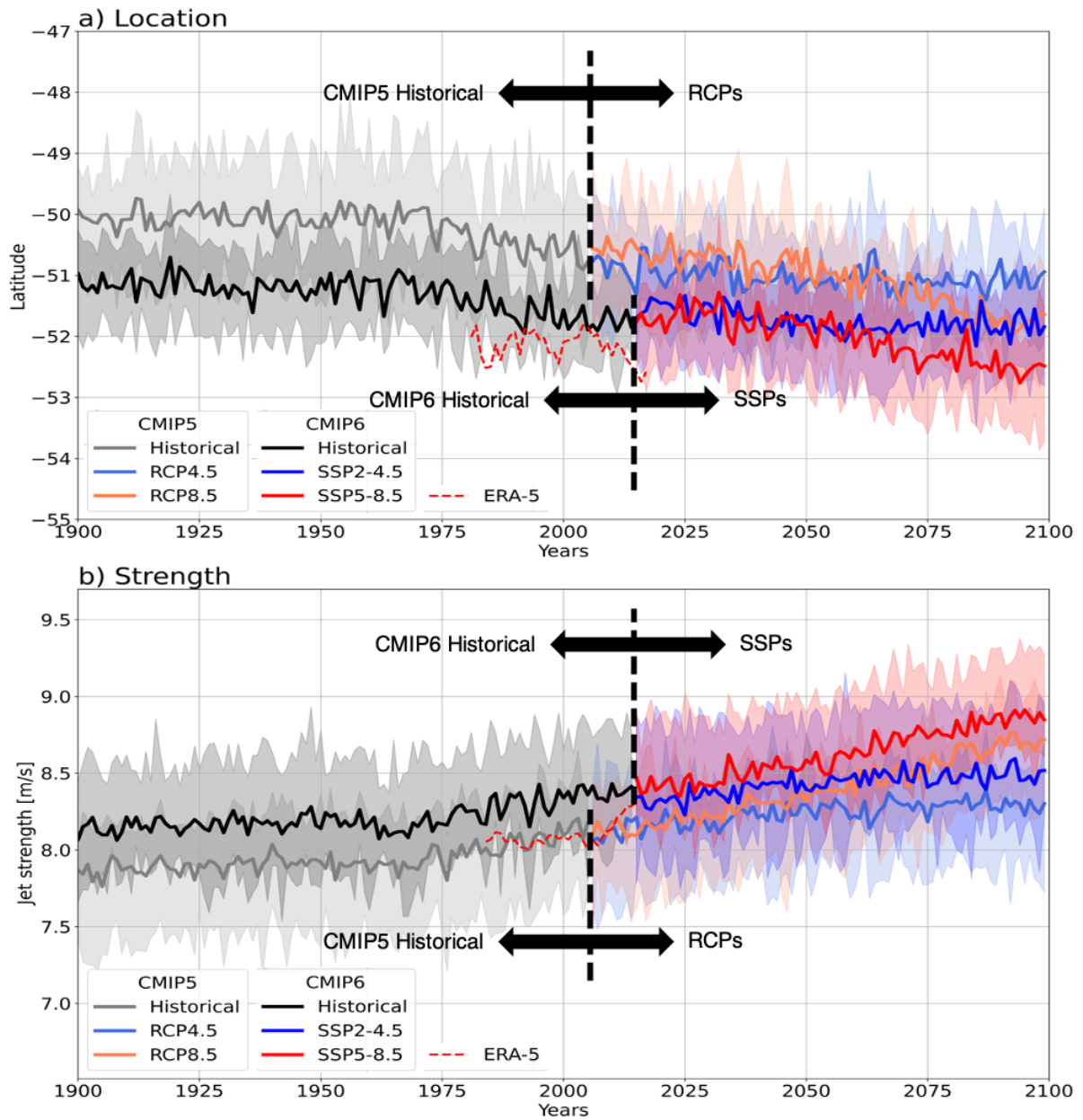
705 Yukimoto, S., Adachi, Y., Hosaka, M., Tomonori, S., Yoshimura, H., Hirabara, M., et al. (2012).
706 A New Global Climate Model of the Meteorological Research Institute: MRI-CGCM3;
707 Model Description and Basic Performance; *Journal of the Meteorological Society of*
708 *Japan*, 90A, 23–64. <https://doi.org/10.2151/jmsj.2012-A02>

709 Yukimoto, S., Hideaki, K., Koshiro, T., Oshima, N., Yoshida, K., Urakawa, S., et al. (2019). The
710 Meteorological Research Institute Earth System Model Version 2.0, MRI-ESM2.0:
711 Description and Basic Evaluation of the Physical Component. *Journal of the*
712 *Meteorological Society of Japan. Ser. II, advpub*. <https://doi.org/10.2151/jmsj.2019-051>

713

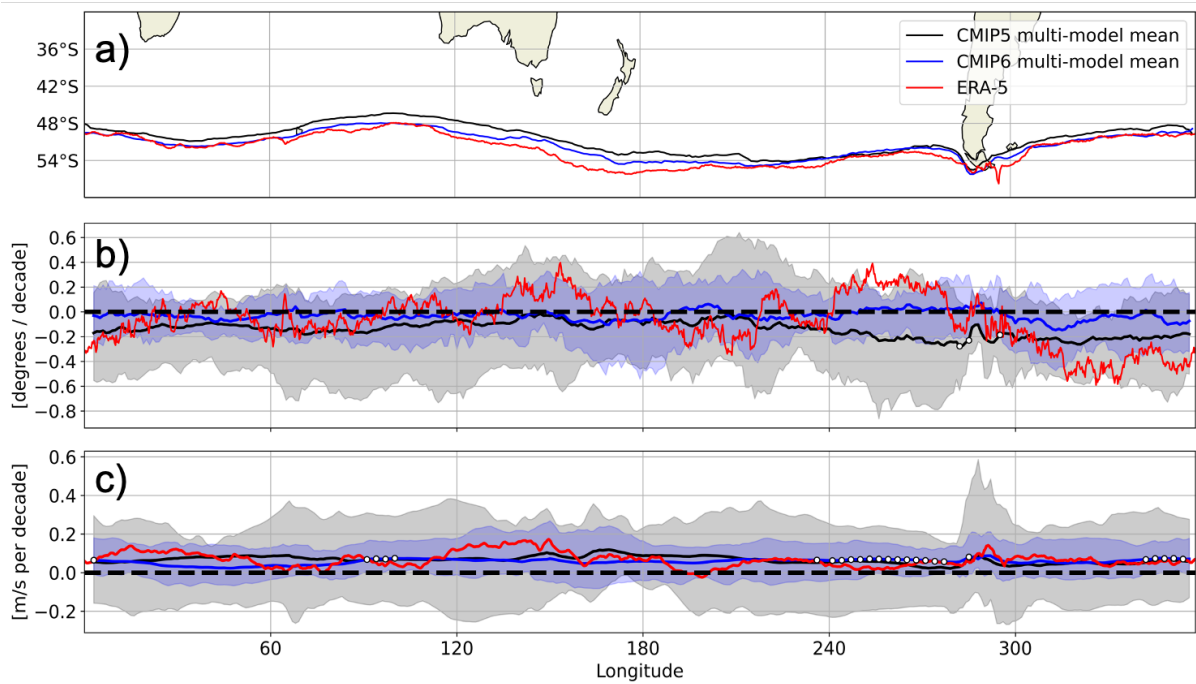
714

715



716

717 **Figure 1** | Position (panel a) and strength (panel b) of maximum Southern Hemisphere
 718 surface westerly winds for CMIP5, CMIP6 models and ERA5. Thick lines represent multi-
 719 model mean and the shading indicates the inter-quartile range based on CMIP5 and CMIP6
 720 ensembles. Red dotted line represents 5-year running mean jet latitude and strength from
 721 the ERA-5 reanalysis from 1979-2019.



722

723 **Figure 2 |** Zonal differences in the wind latitude and strength in CMIP5, CMIP6 and ERA5.

724 Panel a) shows the mean jet position for 2000-2019. Panel b) and c) respectively show the

725 1979-2019 trends in westerly jet shift and strength. Solid black and blue lines in panels b)

726 and c) represent multi-model mean from CMIP5 and CMIP6 respectively and shading

727 represents the inter-quartile range. White circles represent the regions where trends are

728 significant.

729

730

731

732

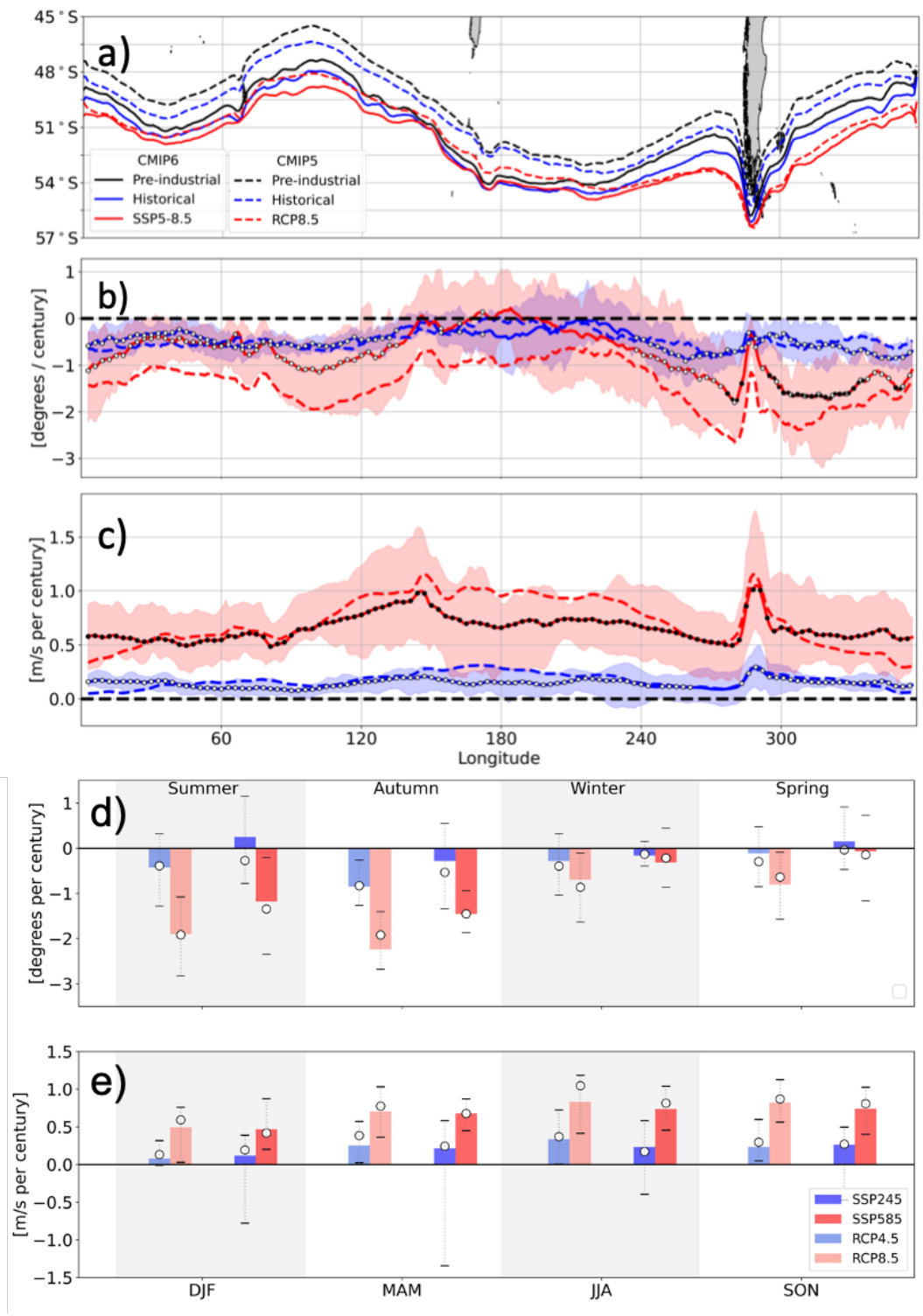
733

734

735

736

737



738

739 **Figure 3** | Past and projected zonal and seasonal differences in wind latitude and strength in
 740 CMIP5 and CMIP6 models. Panel a) shows the multi-model mean jet position during the pre-
 741 industrial scenario (1860-1880 average), historical (1980-1999 average) and SSP5-8.5 (2080-
 742 2099 average). Panel b) and c) respectively show the trends in latitude and strength of

743 westerlies during the 20th (1900-1999) and 21st (2000-2099) Century. Solid lines in panels b)
744 and c) represent multi-model mean and shading represents inter-quartile range from CMIP6
745 models. White circles show the locations where trends are significant. Black dots on solid
746 red lines in panels b) and c) represent the locations where trends during the 21st Century are
747 significantly different from trends during the 20th Century. Panels d) and e) respectively
748 show trends in maximum zonally averaged zonal wind location and strength calculated over
749 2000-2099. Colored bars in panels d) and e) represent multi-model mean trends, circles
750 represent the multi-model median and dashed bars represent the inter-quartile range.

751

Geophysical Research Letters

Supporting Information for

Historical and Projected changes in the Southern Hemisphere surface westerlies

Rishav Goyal^{1,2,*}, Alex Sen Gupta^{1,2}, Martin Jucker^{1,2}, Matthew H. England^{1,2}

1. Climate Change Research Centre, University of New South Wales, NSW, 2052 Australia
2. ARC Centre of Excellence for Climate Extremes, University of New South Wales, NSW, Australia

Contents of this file

Figures S1 to S10

Tables S1 to S3

*Corresponding author: rishav.goyal@unsw.edu.au

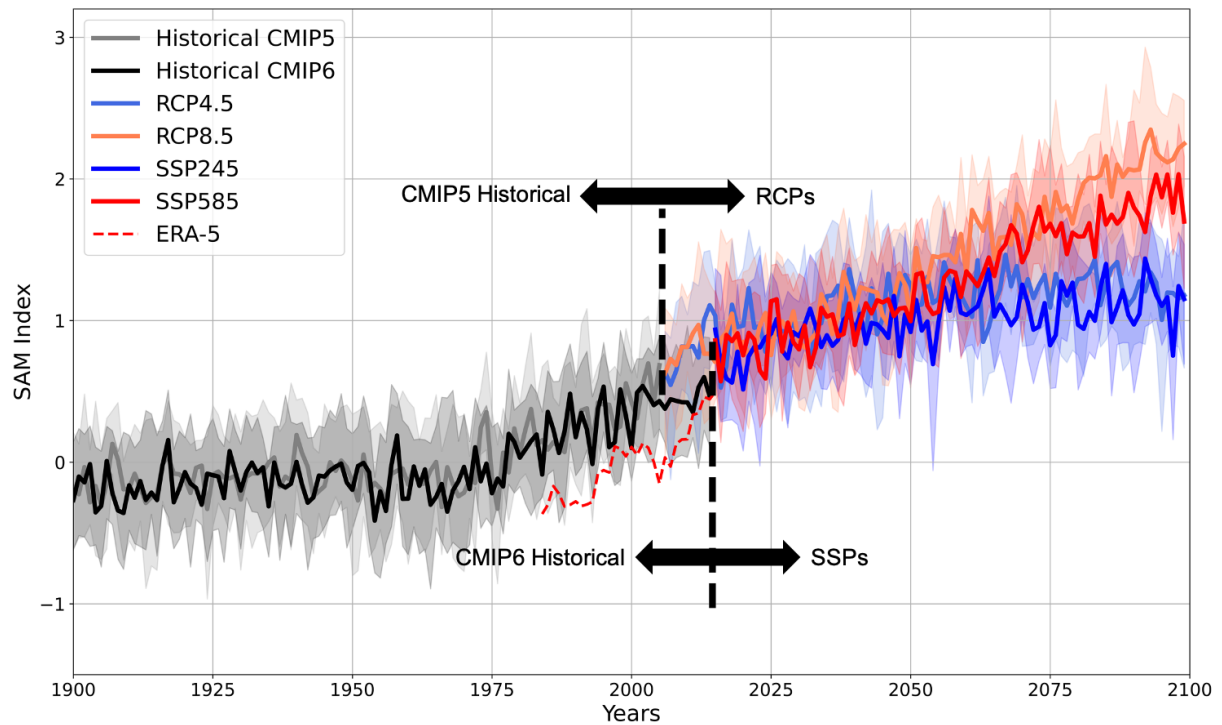


Figure S1 | Southern Annular Mode (SAM) index in CMIP5, CMIP6 models and reanalysis.

SAM index is defined as the difference in the normalized zonal mean sea level pressure between 40°S and 65°S. Thick grey and black lines respectively represent the SAM index for CMIP5 and CMIP6 multi-model mean for historical period (1900-2005 for CMIP5 and 1900-2014 for CMIP6). Thick light blue and orange lines represent the multi-model mean for RCP4.5 and RCP8.5 scenarios of CMIP5 respectively. Thick blue and red lines respectively represent the multi-model mean for SSP245 and SSP585 scenario of CMIP6. Shading around the multi-model mean shows the inter-quartile range from multiple CMIP5 and CMIP6 models. Thin orange line represents 5-year running mean SAM index calculated from ERA-5 reanalysis.

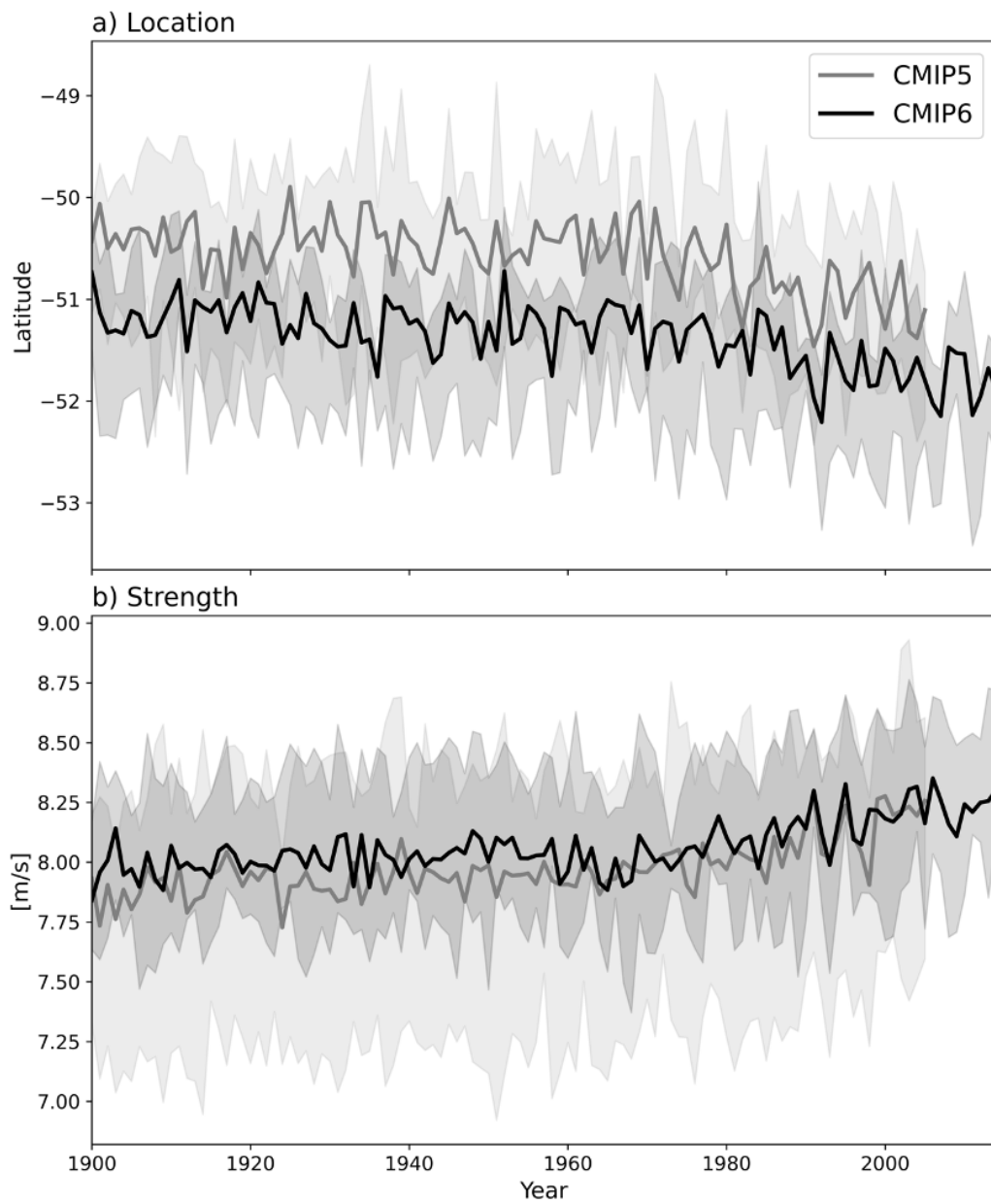


Figure S2 | Zonal mean westerly jet location (panel a) and strength (panel b) in models from common modelling groups from CMIP5 and CMIP6. Details about the models used is given in table S1 and S2.

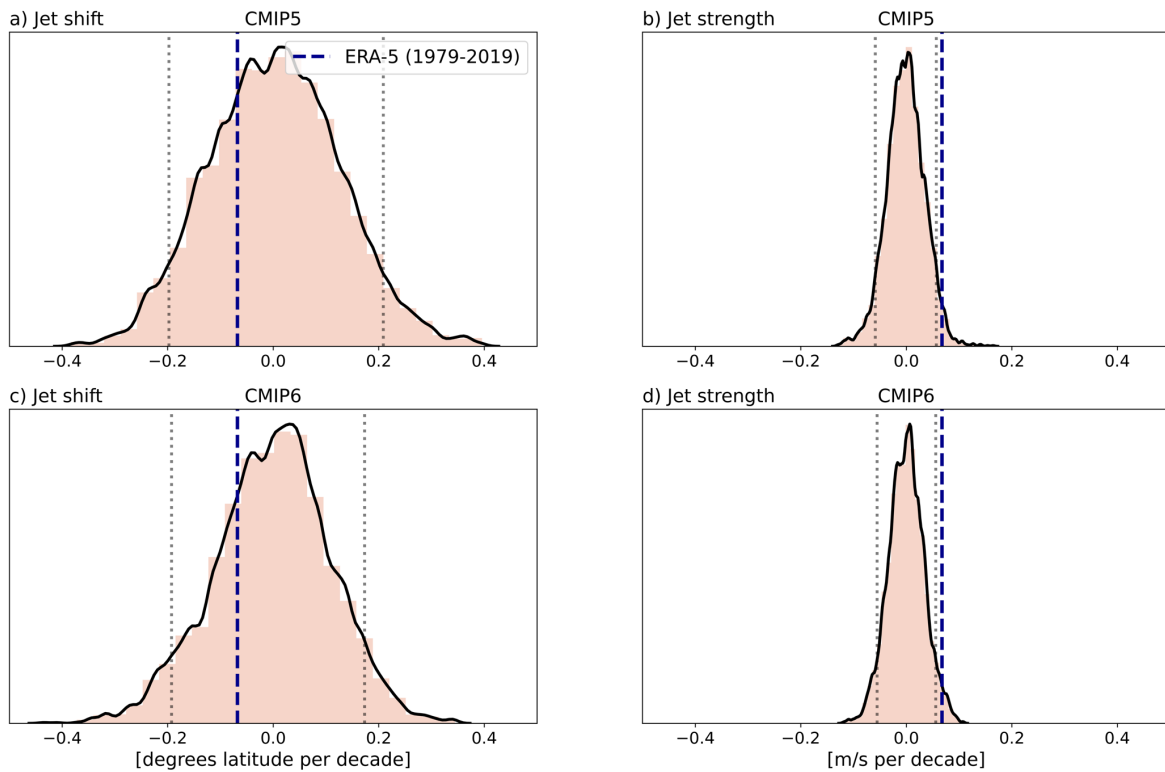


Figure S3 | Histogram represents the probability density function of 41-year annual mean trends calculated from pre-industrial control simulations from 28 CMIP5 and 23 CMIP6 models (200 years for each model). Monte Carlo method is used to calculate the trend over a random chunk of 41 years of data from 200-year simulation of each model and the process is repeated 10,000 times for each model. All the 41-year trends from each model (10,000 for each model) are then concatenated and probability density function is plotted. Dashed blue line represents the trend calculated from ERA5 reanalysis over the current observational time period (1979-2019). Dotted black lines represent 5th and 95th percentile (i.e. bounds for 90% confidence) of the density function. The trends calculated from the reanalysis are significant at 90% confidence if the blue dashed line does not fall between the two dotted black lines.

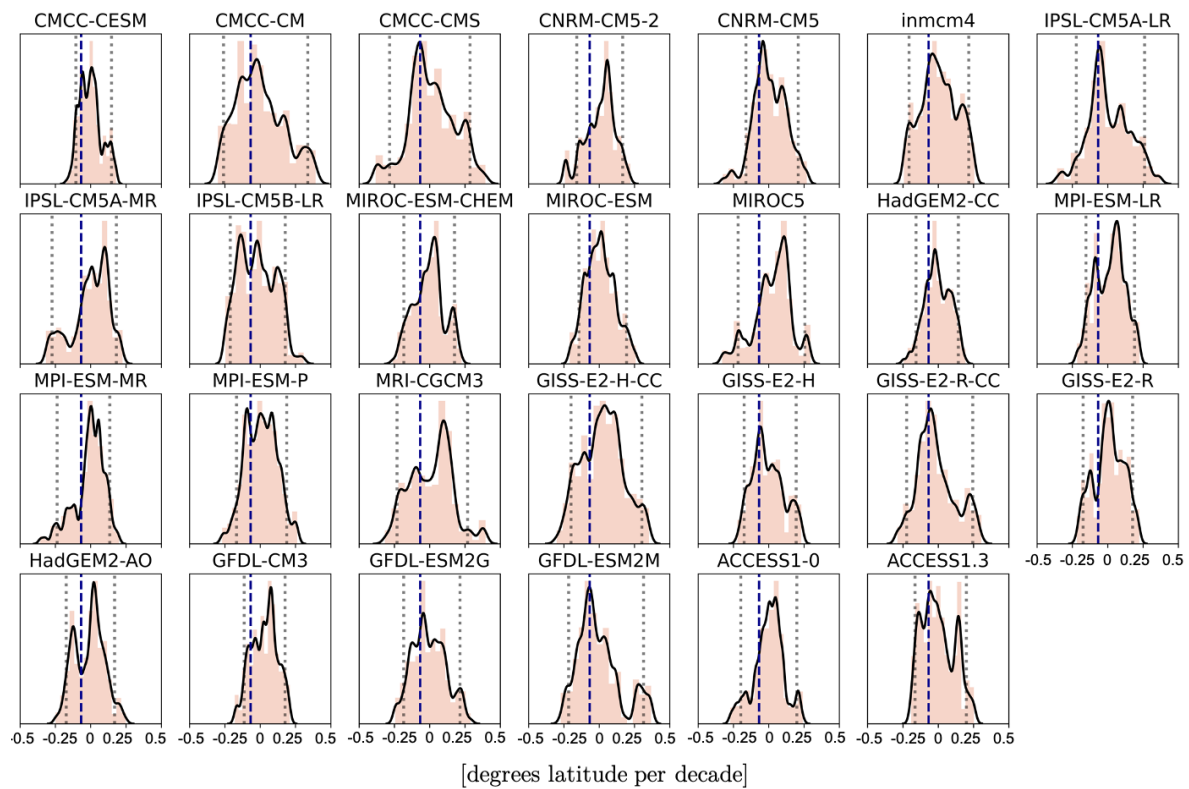


Figure S4 | Histogram represents the probability density function of 41-year annual mean trends in the zonal mean location of SH westerlies calculated from the pre-industrial control simulations from 27 CMIP5 models (200 years for each model). Monte Carlo method is used to calculate the trend over a random chunk of 41 years of data from 200-year simulation of each model and the process is repeated 10,000 times for each model. Dashed blue line represents the trend calculated from ERA5 reanalysis over the current observational time period (1979-2019). Dotted black lines represent 5th and 95th percentile (i.e. bounds for 90% confidence) of the density function. The trends calculated from the reanalysis are significant at 90% confidence if the blue dashed line does not fall between the two dotted black lines.

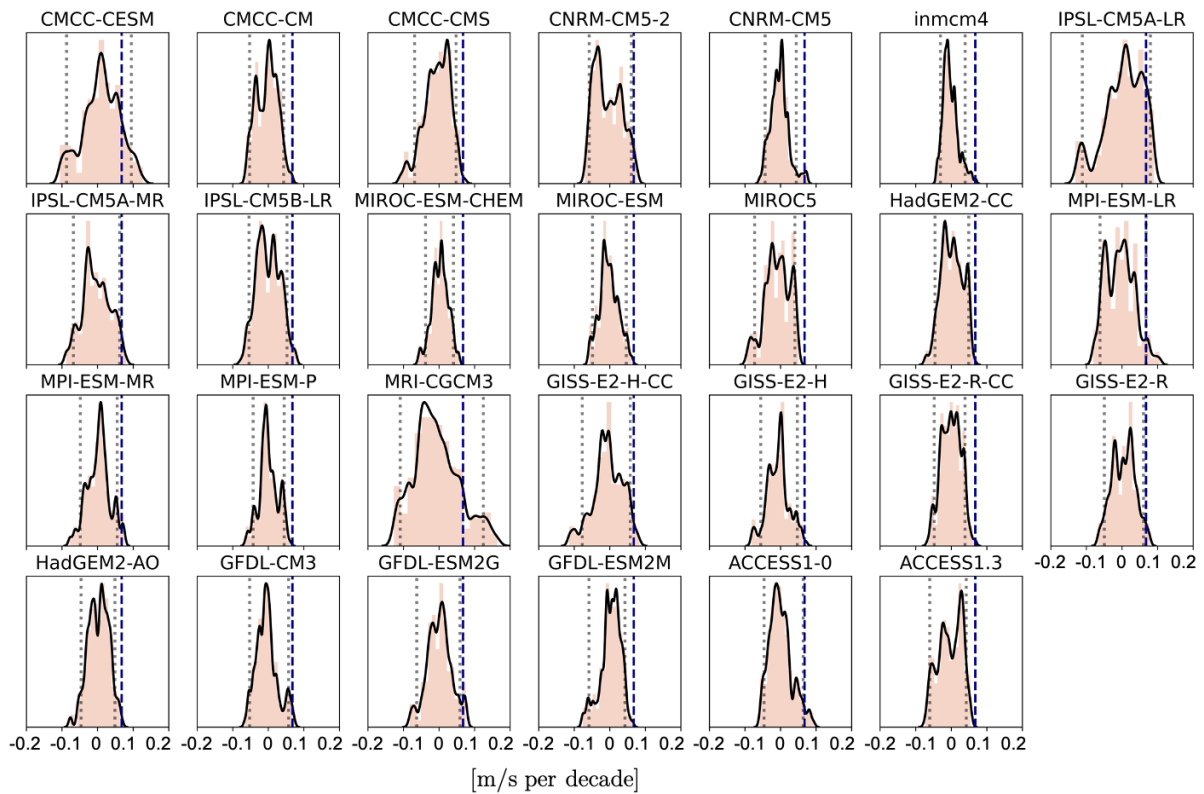


Figure S5 | Histogram represents the probability density function of 41-year annual mean trends in the zonal mean strength of SH westerlies calculated from the pre-industrial control simulations from 27 CMIP5 (200 years for each model). Monte Carlo method is used to calculate the trend over a random chunk of 41 years of data from 200-year simulation of each model and the process is repeated 10,000 times for each model. Dashed blue line represents the trend calculated from ERA5 reanalysis over the current observational time period (1979-2019). Dotted black lines represent 5th and 95th percentile (i.e. bounds for 90% confidence) of the density function. The trends calculated from the reanalysis are significant at 90% confidence if the blue dashed line does not fall between the two dotted black lines.

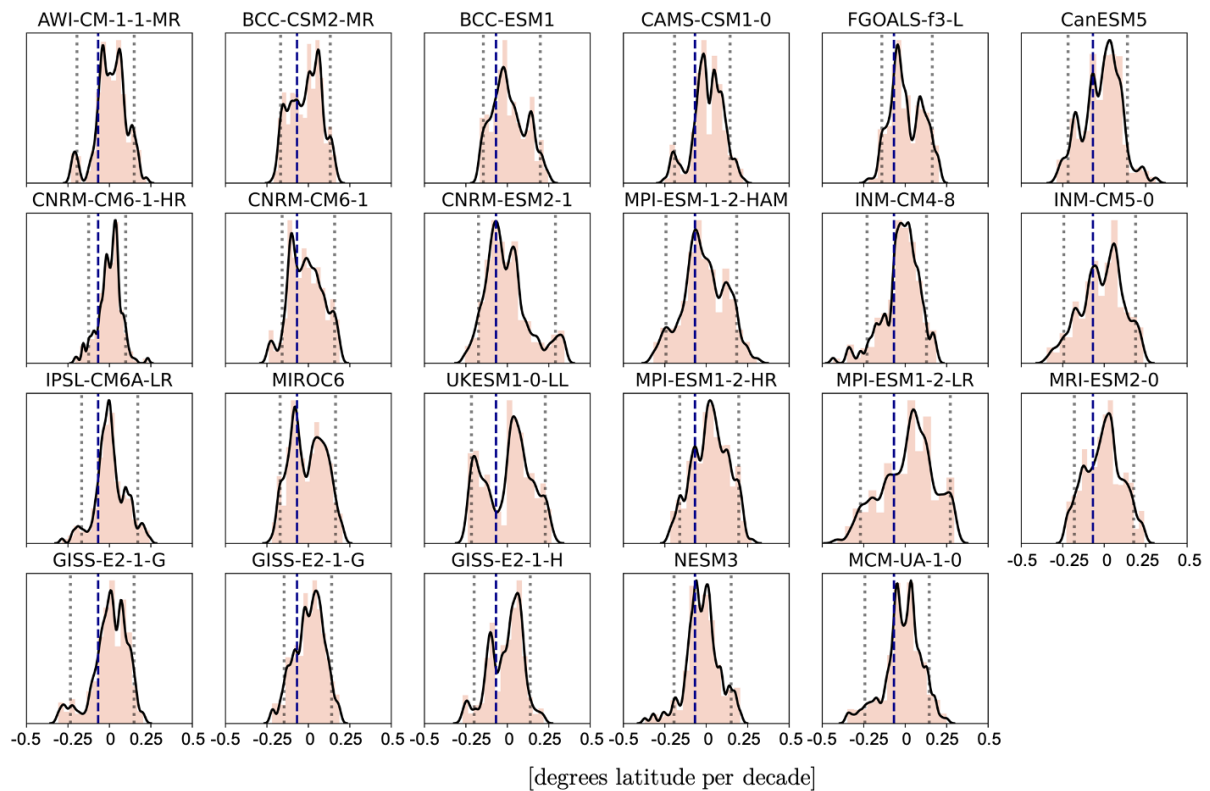


Figure S6 | Histogram represents the probability density function of 41-year annual mean trends in the zonal mean location of SH westerlies calculated from the pre-industrial control simulations from 23 CMIP6 models (200 years for each model). Monte Carlo method is used to calculate the trend over a random chunk of 41 years of data from 200-year simulation of each model and the process is repeated 10,000 times for each model. Dashed blue line represents the trend calculated from ERA5 reanalysis over the current observational time period (1979–2019). Dotted black lines represent 5th and 95th percentile (i.e. bounds for 90% confidence) of the density function. The trends calculated from the reanalysis are significant at 90% confidence if the blue dashed line does not fall between the two dotted black lines.

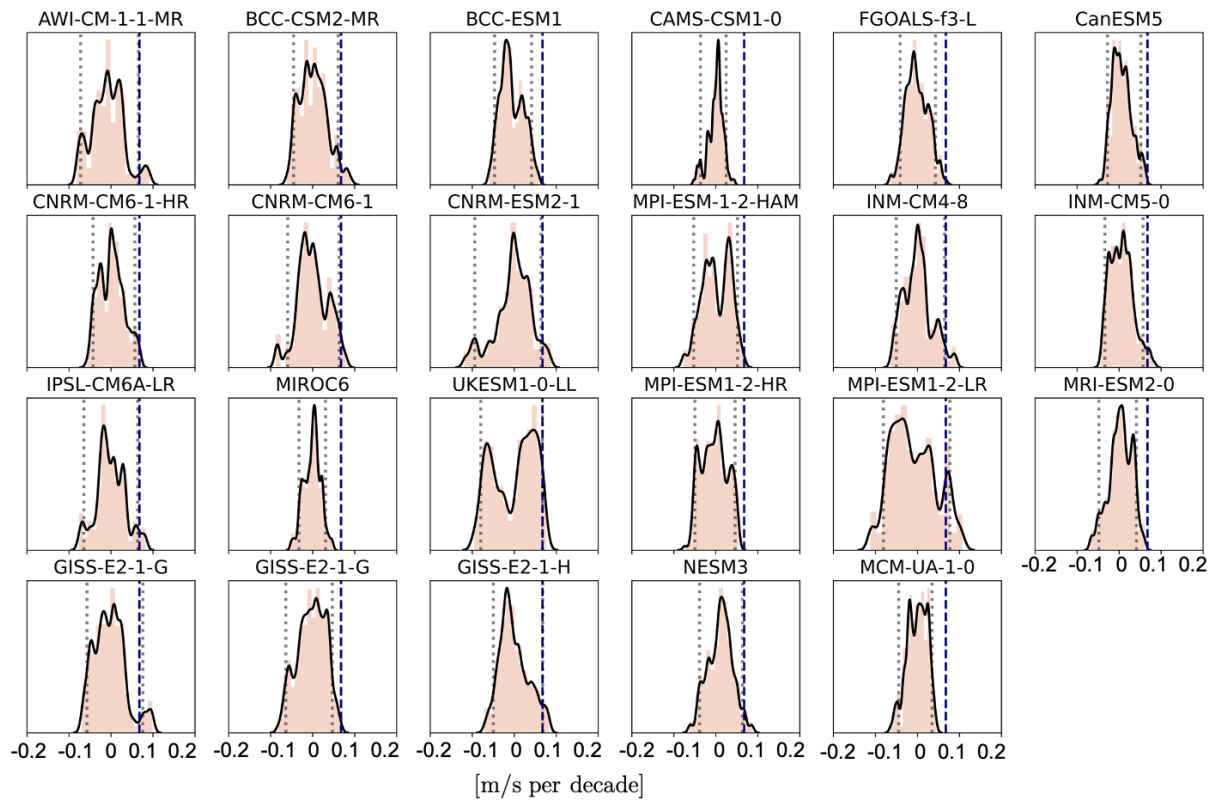


Figure S7 | Histogram represents the probability density function of 41-year annual mean trends in the zonal mean strength of SH westerlies calculated from the pre-industrial control simulations from 23 CMIP6 models (200 years for each model). Monte Carlo method is used to calculate the trend over a random chunk of 41 years of data from 200-year simulation of each model and the process is repeated 10,000 times for each model. Dashed blue line represents the trend calculated from ERA5 reanalysis over the current observational time period (1979-2019). Dotted black lines represent 5th and 95th percentile (i.e. bounds for 90% confidence) of the density function. The trends calculated from the reanalysis are significant at 90% confidence if the blue dashed line does not fall between the two dotted black lines.

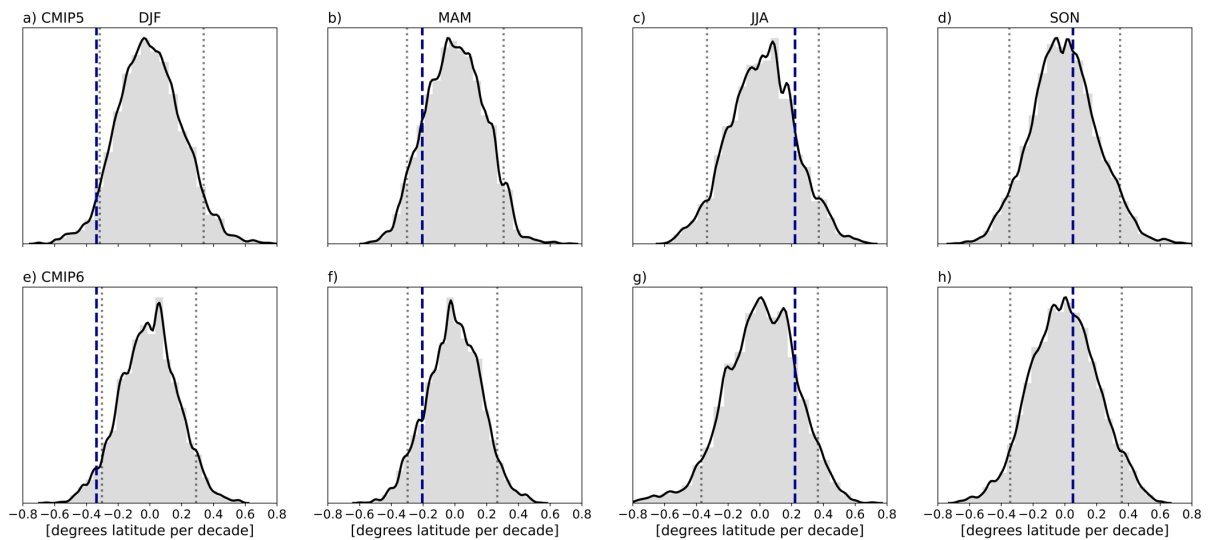


Figure S8 | Histogram represents the probability density function of 41-year trends in the zonal mean location of SH westerlies calculated from pre-industrial control simulations from 28 CMIP5 and 23 CMIP6 models (200 years for each model) for each season. Monte Carlo method is used to calculate the trend over a random chunk of 41 years of data from 200-year simulation of each model and the process is repeated 10,000 times for each model. All the 41-year trends from each model (10,000 for each model) are then concatenated and probability density function is plotted. Dashed blue line represents the trend calculated from ERA5 reanalysis over the current observational time period (1979-2019). Dotted black lines represent 5th and 95th percentile (i.e. bounds for 90% confidence) of the density function. The trends calculated from the reanalysis are significant at 90% confidence if the blue dashed line does not fall between the two dotted black lines.

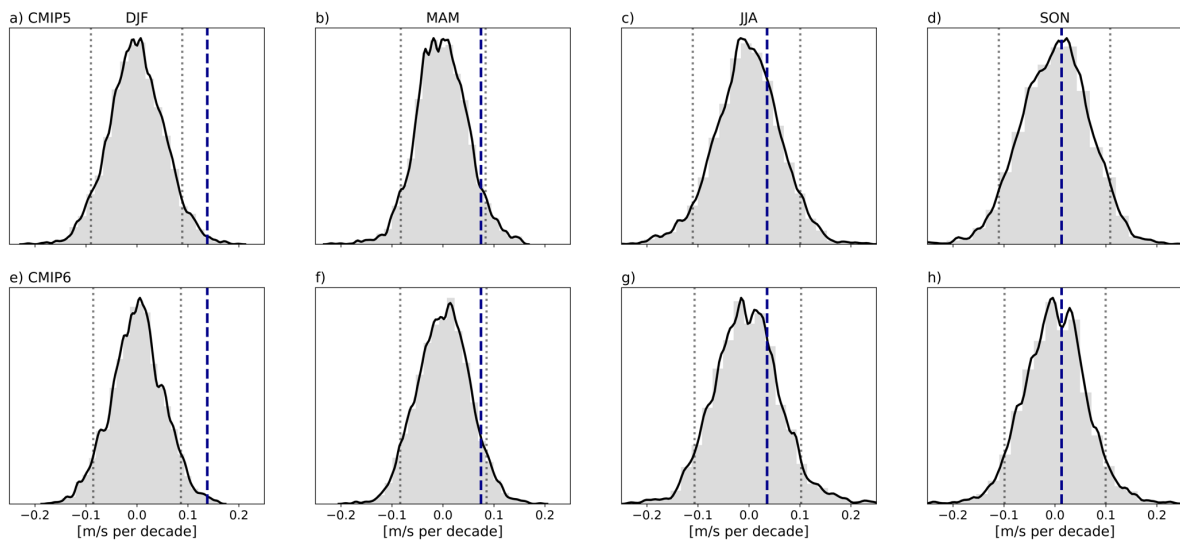


Figure S9 | Histogram represents the probability density function of 41-year trends in the zonal mean strength of SH westerlies calculated from pre-industrial control simulations from 28 CMIP5 and 23 CMIP6 models (200 years for each model) for each season. Monte Carlo method is used to calculate the trend over a random chunk of 41 years of data from 200-year simulation of each model and the process is repeated 10,000 times for each model. All the 41-year trends from each model (10,000 for each model) are then concatenated and probability density function is plotted. Dashed blue line represents the trend calculated from ERA5 reanalysis over the current observational time period (1979-2019). Dotted black lines represent 5th and 95th percentile (i.e. bounds for 90% confidence) of the density function. The trends calculated from the reanalysis are significant at 90% confidence if the blue dashed line does not fall between the two dotted black lines.

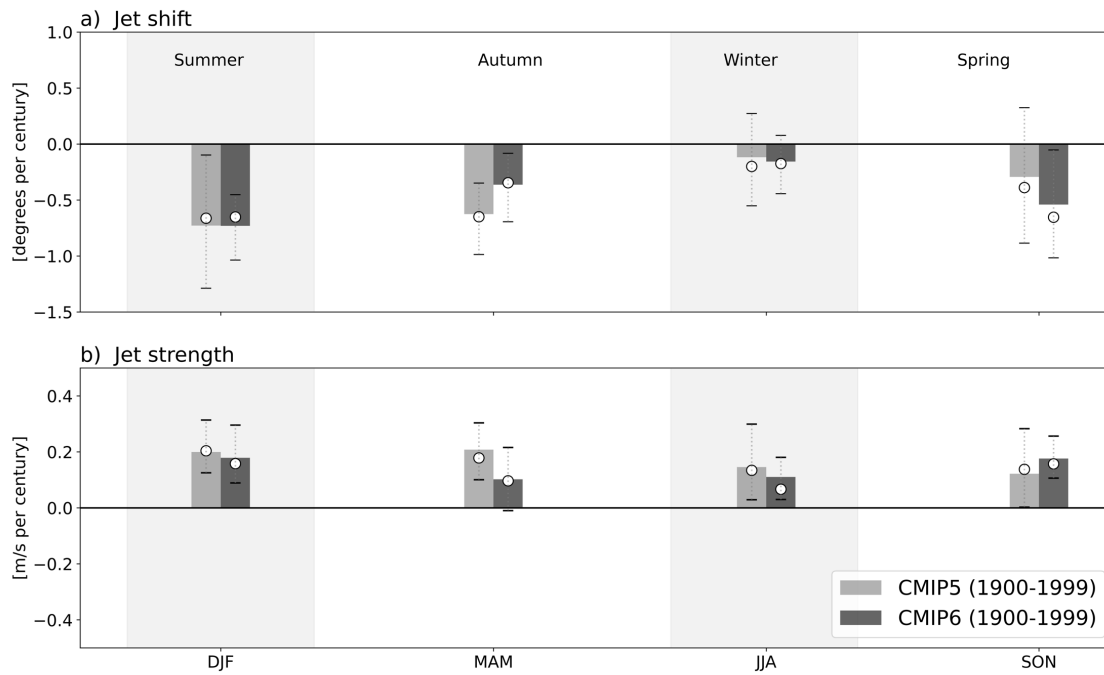


Figure S10 | Historical seasonal trends in position and strength in maximum zonal winds. Trends in maximum zonally averaged zonal wind latitude (panel a) strength (panel b) over historical (1900-1999) for CMIP5 and CMIP6 models. Colored bars represent multi-model mean trends, circles represent the multi-model median and dashed bars represent the inter-quartile range.

Table S1 | CMIP5 models used in the study. Models marked with asterisk are the models used for comparison between CMIP5 and CMIP models

Model	Modeling Center	Scenario			Ozone dataset reference	Main reference
		Historical	RCP4.5	RCP8.5		
CanESM2	Canadian Centre for Climate Modeling and Analysis, Canada	✓	✓	✓	(Cionni et al., 2011)	(von Salzen et al., 2013)
CMCC-CESM	Centro Euro-Mediterraneo sui Cambiamenti Climatici, Italy	✓		✓	(Cionni et al., 2011)	(Vichi et al., 2013)
CMCC-CM		✓	✓	✓	(Cionni et al., 2011)	(Vichi et al., 2013)
CMCC-CMS		✓	✓	✓	(Cionni et al., 2011)	(Vichi et al., 2013)
CNRM-CM5-2	Centre National de Recherches Meteorologiques, France	✓	-	-	(Cariolle & Teyssèdre, 2007)	(Voltaire et al., 2013)
CNRM-CM5		✓	-	-	(Cariolle & Teyssèdre, 2007)	(Voltaire et al., 2013)
INMCM4*	Russian Institute for Numerical Mathematics, Russia	✓	✓	✓	(Cionni et al., 2011)	(E M Volodin et al., 2010)
IPSL-CM5A-LR*	Institut Pierre Simon Laplace, France	✓	✓	✓	(Szopa et al., 2013)	(Dufresne et al., 2013)
IPSL-CM5A-MR		✓	✓	✓	(Szopa et al., 2013)	(Dufresne et al., 2013)
IPSL-CM5B-LR		✓	✓	✓	(Szopa et al., 2013)	(Dufresne et al., 2013)
MIROC-ESM-CHEM	Japan Agency for Marine-Earth Science and Technology, Atmosphere and Ocean Research Institute (The University of Tokyo), and National Institute for Environmental Studies, Japan	✓	✓	✓	(Watanabe et al., 2011)	(Watanabe et al., 2011)
MIROC-ESM		✓		✓	(Watanabe et al., 2011)	(Watanabe et al., 2011)
MIROC5*		✓	✓	✓	(Kawase et al., 2011)	(Watanabe et al., 2011)
HadGEM2-CC	Met Office Hadley Centre, UK	-	✓	✓	(Cionni et al., 2011; Jones et al., 2011)	(Martin et al., 2011)
HadGEM2-ES		-	✓	-	(Jones et al., 2011; O'Connor et al., 2014)	(Collins et al., 2011)
HadCM3		✓	-	-	(Cionni et al., 2011; Jones et al., 2011)	(Gordon et al., 2000)
HadGEM2-AO		✓	✓	✓	(Cionni et al., 2011; Jones et al., 2011)	(Martin et al., 2011)
MPI-ESM-LR*	Max Planck Institute for Meteorology, Germany	✓	-	-	(Cionni et al., 2011; Jones et al., 2011)	(Giorgetta et al., 2013)
MPI-ESM-MR*		✓	✓	✓	(Cionni et al., 2011; Jones et al., 2011)	(Giorgetta et al., 2013)
MPI-ESM-P		✓	-	-	(Cionni et al., 2011; Jones et al., 2011)	(Giorgetta et al., 2013)
MRI-CGCM3	Meteorological Research Institute, Japan Norwegian Climate Centre, Norway	✓	✓	✓	(Cionni et al., 2011)	(Yukimoto et al., 2012)
NorESM1-M*		✓	-	-	(Lamarque et al., 2010, 2012)	(Iversen et al., 2013)
NorESM1-ME		✓	✓		(Lamarque et al., 2010, 2012)	(Iversen et al., 2013)
MRI-ESM1*		✓	-	✓	(Cionni et al., 2011)	(Yukimoto et al., 2012)

GISS-E2-H-CC*	NASA Goddard Institute for Space Studies, USA	✓	✓	✓	(Shindell et al., 2013)	(Schmidt et al., 2006)
GISS-E2-H*		✓	✓	✓	(Hansen et al., 2007)	(Schmidt et al., 2006)
GISS-E2-R-CC		✓	✓	✓	(Shindell et al., 2013)	(Schmidt et al., 2006)
GISS-E2-R*		✓	✓	✓	(Hansen et al., 2007)	(Schmidt et al., 2006)
GFDL-CM2p1	NOAA Geophysical Fluid Dynamics Laboratory, USA	✓	-	-	(Austin & Wilson, 2006; Horowitz et al., 2003)	(Donner et al., 2011)
GFDL-CM3*		✓	✓	✓	(Cionni et al., 2011)	(Donner et al., 2011)
GFDL-ESM2G*		✓	✓	✓	(Cionni et al., 2011)	(Dunne et al., 2012)
GFDL-ESM2M		✓	✓	✓	(Cionni et al., 2011)	(Dunne et al., 2012)
ACCESS1-0	Centre for Australian Weather and Climate Research, Australia	✓	✓	✓	(Cionni et al., 2011)	(Dix et al., 2013)
ACCESS1-3		✓	✓	✓	(Cionni et al., 2011)	(Dix et al., 2013)
CSIRO-Mk-3-6-0	Commonwealth Scientific and Industrial Research Organization in collaboration with Queensland Climate Change Centre of Excellence, Australia	✓	✓	✓	(Cionni et al., 2011)	(Rotstayn et al., 2012)

Table S2 | CMIP6 models used in the study. Models marked with asterisk are the models used for comparison between CMIP5 and CMIP models

Model	Modeling Centre	Scenario			Main reference
		Historical	SSP2-4.5	SSP5-8.5	
AWI-CM-1-1-MR	Alfred Wegener Institute and Helmholtz Centre for Polar and Marine Research, Germany	-	✓	✓	(Semmler et al., 2020)
BCC-CSM2-MR	Beijing Climate Centre, China	✓	✓	✓	(Wu et al., 2019)
BCC-ESM1	Beijing Climate Centre, China	✓	-	-	(Wu et al., 2020)
CAMS-CSM1-0	Chinese Academy of Meteorological Sciences, China	✓	✓	✓	(Rong et al., 2018)
FGOALS-f3-L	Chinese Academy of Sciences, China	-	✓	✓	(He et al., 2019)
CanESM5	Canadian Centre for Climate Modelling and Analysis, Environment and Climate Change Canada, Canada	✓	✓	✓	(Swart et al., 2019)
CNRM-CM6-1-HR	CNRM (Centre National de Recherches Meteorologiques) and CERFACS (Centre Europeen de Recherche et de Formation Avancee en Calcul Scientifique), France	-	✓	✓	(Voldoire et al., 2019)
CNRM-CM6-1		-	✓	✓	(Voldoire et al., 2019)
CNRM-ESM2-1		-	✓		(Séférian et al., 2019)
MPI-ESM-1-2-HAM	ETH Zurich, Switzerland; Max Planck Institut fur Meteorologie, Germany; Forschungszentrum Julich, Germany; University of Oxford, UK; Finnish Meteorological Institute, Finland; Leibniz Institute for Tropospheric Research, Germany; Center for Climate Systems Modeling (C2SM) at ETH Zurich, Switzerland	✓	✓	✓	(Gutjahr et al., 2019)
INM-CM4-8*	Institute for Numerical Mathematics, Russian Academy of Science, Russia	✓	✓	✓	(Evgenii M Volodin et al., 2018)
INM-CM5-0		✓	✓	✓	(E. Volodin & Gritsun, 2018)
IPSL-CM6A-LR*	Institut Pierre Simon Laplace, France	✓	✓	✓	(Boucher et al., 2020)
MIROC6*	JAMSTEC (Japan Agency for Marine-Earth Science and Technology, Japan), AORI (Atmosphere and Ocean Research Institute, The University of Tokyo, Japan), NIES (National Institute for Environmental Studies, Japan), and R-CCS (RIKEN Centre for Computational Science, Japan)	✓	✓	✓	(Tatebe et al., 2019)
MPI-ESM1-2-HR*	Max Planck Institute for Meteorology, Germany; Deutsches Klimarechenzentrum, Germany; Deutscher Wetterdienst, Germany	✓	✓	✓	(Gutjahr et al., 2019)
MPI-ESM1-2-LR*	Max Planck Institute for Meteorology, Germany and Alfred Wegener Institute and Helmholtz Centre for Polar and Marine Research, Germany	✓	✓	✓	(Mauritsen et al., 2019)
MRI-ESM2-0*	Meteorological Research Institute, Japan	✓	✓	-	(Yukimoto et al., 2019)
GISS-E2-1-G-CC*	NASA-GISS (Goddard Institute for Space Studies), USA	✓	-	-	(Bauer et al., 2020)
GISS-E2-1-G*		✓	-	-	
GISS-E2-1-H*		✓	-	-	

NorCPM1*	NorESM Climate modeling Consortium consisting of CICERO (Center for International Climate and Environmental Research), MET-Norway (Norwegian Meteorological Institute), NERSC (Nansen Environmental and Remote Sensing Center), NILU (Norwegian Institute for Air Research), UiB (University of Bergen), UiO (University of Oslo) and UNI (Uni Research), Norway	✓	-	-	(Li et al., 2019)
KACE-1-0-G	National Institute of Meteorological Sciences/Korea Meteorological Administration, Climate Research Division, Republic of Korea	✓	-	-	(Lee et al., 2020)
GFDL-CM4*	National Oceanic and Atmospheric Administration, Geophysical Fluid Dynamics Laboratory, USA	✓	✓	✓	(Held et al., 2019)
GFDL-ESM4*		✓	✓	✓	(Krasting et al., 2018)
NESM3	Nanjing University of Information Science and Technology, China	✓	✓	✓	(Cao et al., 2018)
MCM-UA-1-0	Department of Geosciences, University of Arizona, USA	✓	✓	✓	(Stouffer, 2019)
UKESM1-0-LL	Met Office Hadley Centre, UK; Natural Environment Research Council, UK; National Institute of Meteorological Sciences/Korea Meteorological Administration, Republic of Korea; National Institute of Water and Atmospheric Research, New Zealand	-	✓	✓	(Sellar et al., 2019)

Table S3 | Annual and seasonal trends in the westerly jet shift and strength during the 20th and 21st Century in CMIP5 and CMIP6 models.

Trends are shown as multi-model mean trend \pm one standard deviation. Trends are represented from CMIP5 models (not inside brackets) and from CMIP6 models (inside brackets). Trends in red are from 2000-2099 in RCP8.5 (CMIP5) and SSP5-8.5 (CMIP6) and in blue from 2000-2099 in RCP4.5 (CMIP5) and SSP2-4.5 (CMIP6). Bold values represent trends which are significant at 95% confidence level.

		Annual	DJF	MAM	JJA	SON
1900-1999	Shift (°latitude)	-0.47 \pm 0.37 (-0.46 \pm 0.36)	-0.73 \pm 0.7 (-0.73 \pm 0.53)	-0.63 \pm 0.55 (-0.36 \pm 0.49)	-0.12 \pm 0.58 (-0.16 \pm 0.47)	-0.29 \pm 0.71 (-0.54 \pm 0.77)
	Strength (m/s)	0.17 \pm 0.08 (0.14 \pm 0.09)	0.2 \pm 0.15 (0.18 \pm 0.15)	(0.21 \pm 0.14) (0.10 \pm 0.15)	0.15 \pm 0.16 0.11 \pm 0.13	0.12 \pm 0.21 (0.18 \pm 0.15)
2000-2099	Shift (°latitude)	-1.62 \pm 0.86 (-1.54 \pm 0.82)	-1.9 \pm 1.22 (-1.18 \pm 1.02)	-2.24 \pm 1.22 (-1.45 \pm 1.25)	-0.7 \pm 1.05 (-0.31 \pm 1.17)	-0.81 \pm 1.2 -0.07 \pm 1.6
		-0.56 \pm 0.89 (-0.46 \pm 0.99)	-0.42 \pm 1.29 (0.25 \pm 1.85)	-0.85 \pm 0.92 -0.28 \pm 1.38	-0.28 \pm 0.97 (-0.16 \pm 0.99)	-0.11 \pm 1.09 0.15 \pm 1.34
	Strength (m/s)	0.79 \pm 0.52 (0.66 \pm 0.46)	0.49 \pm 0.56 (0.47 \pm 0.43)	0.70 \pm 0.51 (0.68 \pm 0.43)	0.83 \pm 0.6 (0.74 \pm 0.64)	0.82 \pm 0.60 0.74 \pm 0.53
		0.24 \pm 0.37 (0.21 \pm 0.46)	0.08 \pm 0.48 0.12 \pm 0.39	0.25 \pm 0.50 (0.22 \pm 0.48)	0.34 \pm 0.46 (0.23 \pm 0.62)	0.24 \pm 0.47 0.27 \pm 0.50

References

- Austin, J., & Wilson, R. J. (2006). Ensemble simulations of the decline and recovery of stratospheric ozone. *Journal of Geophysical Research: Atmospheres*, *111*(D16).
<https://doi.org/10.1029/2005JD006907>
- Bauer, S. E., Tsigaridis, K., Faluvegi, G., Kelley, M., Lo, K. K., Miller, R. L., et al. (2020). Historical (1850-2014) aerosol evolution and role on climate forcing using the GISS ModelE2.1 contribution to CMIP6. *Journal of Advances in Modeling Earth Systems*, e2019MS001978. <https://doi.org/10.1029/2019MS001978>
- Boucher, O., Servonnat, J., Albright, A. L., Aumont, O., Balkanski, Y., Bastrikov, V., et al. (2020). Presentation and evaluation of the IPSL-CM6A-LR climate model. *Journal of Advances in Modeling Earth Systems*, e2019MS002010.
<https://doi.org/10.1029/2019MS002010>
- Cao, J., Wang, B., Yang, Y.-M., Ma, L., Li, J., Sun, B., et al. (2018). The NUIST Earth System Model (NESM) version 3: description and preliminary evaluation. *Geosci. Model Dev.*, *11*(7), 2975–2993. <https://doi.org/10.5194/gmd-11-2975-2018>
- Cariolle, D., & Teyssèdre, H. (2007). A revised linear ozone photochemistry parameterization for use in transport and general circulation models: multi-annual simulations. *Atmos. Chem. Phys.*, *7*(9), 2183–2196. <https://doi.org/10.5194/acp-7-2183-2007>
- Cionni, I., Eyring, V., Lamarque, J. F., Randel, W. J., Stevenson, D. S., Wu, F., et al. (2011). Ozone database in support of CMIP5 simulations: Results and corresponding radiative forcing. *Atmospheric Chemistry and Physics*, *11*(21), 11267–11292.
<https://doi.org/10.5194/acp-11-11267-2011>
- Collins, W. J., Bellouin, N., Doutriaux-Boucher, M., Gedney, N., Halloran, P., Hinton, T., et al. (2011). Development and evaluation of an Earth-System model – HadGEM2. *Geosci.*

Model Dev., 4(4), 1051–1075. <https://doi.org/10.5194/gmd-4-1051-2011>

Dix, M., Vohralik, P., Bi, D., Rashid, H., Marsland, S., O'Farrell, S., et al. (2013). The ACCESS coupled model: Documentation of core CMIP5 simulations and initial results. *Australian Meteorological and Oceanographic Journal*, 63(1), 83–99.
<https://doi.org/10.22499/2.6301.006>

Donner, L. J., Wyman, B. L., Hemler, R. S., Horowitz, L. W., Ming, Y., Zhao, M., et al. (2011). The Dynamical Core, Physical Parameterizations, and Basic Simulation Characteristics of the Atmospheric Component AM3 of the GFDL Global Coupled Model CM3. *Journal of Climate*, 24(13), 3484–3519. <https://doi.org/10.1175/2011JCLI3955.1>

Dufresne, J.-L., Foujols, M.-A., Denvil, S., Caubel, A., Marti, O., Aumont, O., et al. (2013). Climate change projections using the IPSL-CM5 Earth System Model: from CMIP3 to CMIP5. *Climate Dynamics*, 40(9), 2123–2165. <https://doi.org/10.1007/s00382-012-1636-1>

Dunne, J. P., John, J. G., Adcroft, A. J., Griffies, S. M., Hallberg, R. W., Shevliakova, E., et al. (2012). GFDL's ESM2 Global Coupled Climate–Carbon Earth System Models. Part I: Physical Formulation and Baseline Simulation Characteristics. *Journal of Climate*, 25(19), 6646–6665. <https://doi.org/10.1175/JCLI-D-11-00560.1>

Giorgetta, M. A., Jungclaus, J., Reick, C. H., Legutke, S., Bader, J., Böttinger, M., et al. (2013). Climate and carbon cycle changes from 1850 to 2100 in MPI-ESM simulations for the Coupled Model Intercomparison Project phase 5. *Journal of Advances in Modeling Earth Systems*, 5(3), 572–597. <https://doi.org/10.1002/jame.20038>

Gordon, C., Cooper, C., Senior, C. A., Banks, H., Gregory, J. M., Johns, T. C., et al. (2000). The simulation of SST, sea ice extents and ocean heat transports in a version of the Hadley Centre coupled model without flux adjustments. *Climate Dynamics*, 16(2), 147–168.

<https://doi.org/10.1007/s003820050010>

Gutjahr, O., Putrasahan, D., Lohmann, K., Jungclaus, J. H., von Storch, J.-S., Brüggemann, N., et al. (2019). Max Planck Institute Earth System Model (MPI-ESM1.2) for the High-Resolution Model Intercomparison Project (HighResMIP). *Geosci. Model Dev.*, *12*(7), 3241–3281. <https://doi.org/10.5194/gmd-12-3241-2019>

Hansen, J., Sato, M., Ruedy, R., Kharecha, P., Lacis, A., Miller, R., et al. (2007). Climate simulations for 1880–2003 with GISS modelE. *Climate Dynamics*, *29*(7), 661–696. <https://doi.org/10.1007/s00382-007-0255-8>

He, B., Bao, Q., Wang, X., Zhou, L., Wu, X., Liu, Y., et al. (2019). CAS FGOALS-f3-L Model Datasets for CMIP6 Historical Atmospheric Model Intercomparison Project Simulation. *Advances in Atmospheric Sciences*, *36*(8), 771–778. <https://doi.org/10.1007/s00376-019-9027-8>

Held, I. M., Guo, H., Adcroft, A., Dunne, J. P., Horowitz, L. W., Krasting, J., et al. (2019). Structure and Performance of GFDL's CM4.0 Climate Model. *Journal of Advances in Modeling Earth Systems*, *11*(11), 3691–3727. <https://doi.org/10.1029/2019MS001829>

Horowitz, L. W., Walters, S., Mauzerall, D. L., Emmons, L. K., Rasch, P. J., Granier, C., et al. (2003). A global simulation of tropospheric ozone and related tracers: Description and evaluation of MOZART, version 2. *Journal of Geophysical Research: Atmospheres*, *108*(D24). <https://doi.org/10.1029/2002JD002853>

Iversen, T., Bentsen, M., Bethke, I., Debernard, J. B., Kirkevåg, A., Seland, Ø., et al. (2013). The Norwegian Earth System Model, NorESM1-M – Part 2: Climate response and scenario projections. *Geosci. Model Dev.*, *6*(2), 389–415. <https://doi.org/10.5194/gmd-6-389-2013>

Jones, C. D., Hughes, J. K., Bellouin, N., Hardiman, S. C., Jones, G. S., Knight, J., et al. (2011).

- The HadGEM2-ES implementation of CMIP5 centennial simulations. *Geosci. Model Dev.*, 4(3), 543–570. <https://doi.org/10.5194/gmd-4-543-2011>
- Kawase, H., Nagashima, T., Sudo, K., & Nozawa, T. (2011). Future changes in tropospheric ozone under Representative Concentration Pathways (RCPs). *Geophysical Research Letters*, 38(5). <https://doi.org/10.1029/2010GL046402>
- Krasting, J. P., John, J. G., Blanton, C., McHugh, C., Nikonov, S., Radhakrishnan, A., et al. (2018). NOAA-GFDL GFDL-ESM4 model output prepared for CMIP6 CMIP historical. Earth System Grid Federation. <https://doi.org/10.22033/ESGF/CMIP6.8597>
- Lamarque, J.-F., Bond, T. C., Eyring, V., Granier, C., Heil, A., Klimont, Z., et al. (2010). Historical (1850–2000) gridded anthropogenic and biomass burning emissions of reactive gases and aerosols: methodology and application. *Atmos. Chem. Phys.*, 10(15), 7017–7039. <https://doi.org/10.5194/acp-10-7017-2010>
- Lamarque, J.-F., Emmons, L. K., Hess, P. G., Kinnison, D. E., Tilmes, S., Vitt, F., et al. (2012). CAM-chem: description and evaluation of interactive atmospheric chemistry in the Community Earth System Model. *Geosci. Model Dev.*, 5(2), 369–411. <https://doi.org/10.5194/gmd-5-369-2012>
- Lee, J., Kim, J., Sun, M.-A., Kim, B.-H., Moon, H., Sung, H. M., et al. (2020). Evaluation of the Korea Meteorological Administration Advanced Community Earth-System model (K-ACE). *Asia-Pacific Journal of Atmospheric Sciences*, 56(3), 381–395. <https://doi.org/10.1007/s13143-019-00144-7>
- Li, F., Orsolini, Y. J., Keenlyside, N., Shen, M.-L., Counillon, F., & Wang, Y. G. (2019). Impact of Snow Initialization in Subseasonal-to-Seasonal Winter Forecasts With the Norwegian Climate Prediction Model. *Journal of Geophysical Research: Atmospheres*, 124(17–18), 10033–10048. <https://doi.org/10.1029/2019JD030903>

- Martin, G. M., Bellouin, N., Collins, W. J., Culverwell, I. D., Halloran, P. R., Hardiman, S. C., et al. (2011). The HadGEM2 family of Met Office Unified Model climate configurations. *Geoscientific Model Development*, 4(3), 723–757. <https://doi.org/10.5194/gmd-4-723-2011>
- Mauritsen, T., Bader, J., Becker, T., Behrens, J., Bittner, M., Brokopf, R., et al. (2019). Developments in the MPI-M Earth System Model version 1.2 (MPI-ESM1.2) and Its Response to Increasing CO₂. *Journal of Advances in Modeling Earth Systems*, 11(4), 998–1038. <https://doi.org/10.1029/2018MS001400>
- O'Connor, F. M., Johnson, C. E., Morgenstern, O., Abraham, N. L., Braesicke, P., Dalvi, M., et al. (2014). Evaluation of the new UKCA climate-composition model – Part 2: The Troposphere. *Geosci. Model Dev.*, 7(1), 41–91. <https://doi.org/10.5194/gmd-7-41-2014>
- Rong, X., Li, J., Chen, H., Xin, Y., Su, J., Hua, L., et al. (2018). The CAMS Climate System Model and a Basic Evaluation of Its Climatology and Climate Variability Simulation. *Journal of Meteorological Research*, 32(6), 839–861. <https://doi.org/10.1007/s13351-018-8058-x>
- Rotstayn, L. D., Jeffrey, S. J., Collier, M. A., Dravitzki, S. M., Hirst, A. C., Syktus, J. I., & Wong, K. K. (2012). Aerosol- and greenhouse gas-induced changes in summer rainfall and circulation in the Australasian region: a study using single-forcing climate simulations. *Atmos. Chem. Phys.*, 12(14), 6377–6404. <https://doi.org/10.5194/acp-12-6377-2012>
- von Salzen, K., Scinocca, J. F., McFarlane, N. A., Li, J., Cole, J. N. S., Plummer, D., et al. (2013). The Canadian Fourth Generation Atmospheric Global Climate Model (CanAM4). Part I: Representation of Physical Processes. *Atmosphere-Ocean*, 51(1), 104–125. <https://doi.org/10.1080/07055900.2012.755610>
- Schmidt, G. A., Ruedy, R., Hansen, J. E., Aleinov, I., Bell, N., Bauer, M., et al. (2006). Present-Day Atmospheric Simulations Using GISS ModelE: Comparison to In Situ, Satellite, and

Reanalysis Data. *Journal of Climate*, 19(2), 153–192.

<https://doi.org/10.1175/JCLI3612.1>

Séférian, R., Nabat, P., Michou, M., Saint-Martin, D., Voldoire, A., Colin, J., et al. (2019).

Evaluation of CNRM Earth System Model, CNRM-ESM2-1: Role of Earth System Processes in Present-Day and Future Climate. *Journal of Advances in Modeling Earth Systems*, 11(12), 4182–4227. <https://doi.org/10.1029/2019MS001791>

Sellar, A. A., Jones, C. G., Mulcahy, J. P., Tang, Y., Yool, A., Wiltshire, A., et al. (2019).

UKESM1: Description and Evaluation of the U.K. Earth System Model. *Journal of Advances in Modeling Earth Systems*, 11(12), 4513–4558.

<https://doi.org/10.1029/2019MS001739>

Semmler, A.-T., Danilov, S., Gierz, P., Goessling, H., Hegewald, J., Hinrichs, C., et al. (2020).

Simulations for CMIP6 with the AWI climate model AWI-CM-1-1. *Earth and Space Science Open Archive*. <https://doi.org/10.1002/essoar.10501538.1>

Shindell, D. T., Pechony, O., Voulgarakis, A., Faluvegi, G., Nazarenko, L., Lamarque, J.-F., et

al. (2013). Interactive ozone and methane chemistry in GISS-E2 historical and future climate simulations. *Atmos. Chem. Phys.*, 13(5), 2653–2689.

<https://doi.org/10.5194/acp-13-2653-2013>

Stouffer, R. (2019). U of Arizona MCM-UA-1-0 model output prepared for CMIP6 CMIP.

Earth System Grid Federation. <https://doi.org/10.22033/ESGF/CMIP6.2421>

Swart, N. C., Cole, J. N. S., Kharin, V. V., Lazare, M., Scinocca, J. F., Gillett, N. P., et al. (2019).

The Canadian Earth System Model version 5 (CanESM5.0.3). *Geosci. Model Dev.*, 12(11), 4823–4873. <https://doi.org/10.5194/gmd-12-4823-2019>

Szopa, S., Balkanski, Y., Schulz, M., Bekki, S., Cugnet, D., Fortems-Cheiney, A., et al. (2013).

Aerosol and ozone changes as forcing for climate evolution between 1850 and 2100.

- Climate Dynamics*, 40(9), 2223–2250. <https://doi.org/10.1007/s00382-012-1408-y>
- Tatebe, H., Ogura, T., Nitta, T., Komuro, Y., Ogochi, K., Takemura, T., et al. (2019). Description and basic evaluation of simulated mean state, internal variability, and climate sensitivity in MIROC6. *Geosci. Model Dev.*, 12(7), 2727–2765. <https://doi.org/10.5194/gmd-12-2727-2019>
- Vichi, M., Navarra, A., & Fogli, P. G. (2013). Adjustment of the natural ocean carbon cycle to negative emission rates. *Climatic Change*, 118(1), 105–118. <https://doi.org/10.1007/s10584-012-0677-0>
- Voldoire, A., Sanchez-Gomez, E., Salas y Mélia, D., Decharme, B., Cassou, C., Sénési, S., et al. (2013). The CNRM-CM5.1 global climate model: description and basic evaluation. *Climate Dynamics*, 40(9), 2091–2121. <https://doi.org/10.1007/s00382-011-1259-y>
- Voldoire, A., Saint-Martin, D., Sénési, S., Decharme, B., Alias, A., Chevallier, M., et al. (2019). Evaluation of CMIP6 DECK Experiments With CNRM-CM6-1. *Journal of Advances in Modeling Earth Systems*, 11(7), 2177–2213. <https://doi.org/10.1029/2019MS001683>
- Volodin, E., & Gritsun, A. (2018). Simulation of observed climate changes in 1850-2014 with climate model INM-CM5. *Earth System Dynamics*, 9(4), 1235–1242. <https://doi.org/10.5194/esd-9-1235-2018>
- Volodin, E M, Dianskii, N. A., & Gusev, A. V. (2010). Simulating present-day climate with the INMCM4.0 coupled model of the atmospheric and oceanic general circulations. *Izvestiya, Atmospheric and Oceanic Physics*, 46(4), 414–431. <https://doi.org/10.1134/S000143381004002X>
- Volodin, Evgenii M, Mortikov, E. V, Kostykin, S. V, Galin, V. Y., Lykossov, V. N., Gritsun, A. S., et al. (2018). Simulation of the modern climate using the INM-CM48 climate model. *Russian Journal of Numerical Analysis and Mathematical Modelling*, 33(6), 367–374.

<https://doi.org/https://doi.org/10.1515/rnam-2018-0032>

Watanabe, S., Hajima, T., Sudo, K., Nagashima, T., Takemura, T., Okajima, H., et al. (2011).

MIROC-ESM 2010: model description and basic results of CMIP5-20c3m experiments.

Geosci. Model Dev., 4(4), 845–872. <https://doi.org/10.5194/gmd-4-845-2011>

Wu, T., Lu, Y., Fang, Y., Xin, X., Li, L., Li, W., et al. (2019). The Beijing Climate Center Climate

System Model (BCC-CSM): The main progress from CMIP5 to CMIP6. *Geoscientific*

Model Development, 12(4), 1573–1600. <https://doi.org/10.5194/gmd-12-1573-2019>

Wu, T., Zhang, F., Zhang, J., Jie, W., Zhang, Y., Wu, F., et al. (2020). Beijing Climate Center

Earth System Model version 1 (BCC-ESM1): Model description and evaluation of

aerosol simulations. *Geoscientific Model Development*, 13(3), 977–1005.

<https://doi.org/10.5194/gmd-13-977-2020>

Yukimoto, S., Adachi, Y., Hosaka, M., Tomonori, S., Yoshimura, H., Hirabara, M., et al. (2012).

A New Global Climate Model of the Meteorological Research Institute: MRI-CGCM3:

Model Description and Basic Performance. *Journal of the Meteorological Society of*

Japan, 90A, 23–64. <https://doi.org/10.2151/jmsj.2012-A02>

Yukimoto, S., Hideaki, K., Koshiro, T., Oshima, N., Yoshida, K., Urakawa, S., et al. (2019). The

Meteorological Research Institute Earth System Model Version 2.0, MRI-ESM2.0:

Description and Basic Evaluation of the Physical Component. *Journal of the*

Meteorological Society of Japan. Ser. II, advpub. <https://doi.org/10.2151/jmsj.2019-051>